

Inverse mass cascade of self-gravitating collisionless flow and effects on  
halo deformation, energy, size, and density profiles

Zhijie (Jay) Xu<sup>1,a</sup>

1. Computational Mathematics Group, Physical and Computational Sciences Directorate, Pacific  
Northwest National Laboratory, Richland, WA 99352, USA

Abstract:

The inverse mass cascade is a key feature of the intermediate statistically steady state of self-gravitating collisionless flow (SG-CFD). Mass cascade is local, two-way, and asymmetric in mass space. Halos inherit/pass their mass mostly from/to halos of similar size. The net mass transfer proceeds in a “bottom-up” fashion. This paper focus on the effects of inverse mass cascade on halo energy, momentum, size, and internal structure. Halos with fast mass accretion have an expanding core proportional to their growing size. Mass cascade forms a new layer of mass that deforms the original halo and induces a nonzero radial flow (outwards for core and inwards for outer regions). Halo density profile can be determined by correct modeling of radial flow. An isothermal profile has a vanishing radial flow. The inward/outward flow leads to an extra length scale (scale radius where radial flow is at maximum) that is not present in isothermal profile. A limiting value of concentration  $c=3.5$  can be explicitly derived for fast growing halos with a vanishing momentum. To provide insights into the cusp-core controversy, a double-power-law density is proposed as a natural result of nonzero radial flow. The inner density is controlled by halo deformation rate, while outer density is controlled by halo growth from mass cascade. The slower deformation at halo center leads to a steeper density profile. For halos with fast mass accretion, the radial flow at center is simply a Hubble flow that leads to the existence of a central core.

---

<sup>a)</sup> Electronic mail: [zhijie.xu@pnnl.gov](mailto:zhijie.xu@pnnl.gov); [zhijiexu@hotmail.com](mailto:zhijiexu@hotmail.com)

The velocity dispersion of non-rotating halos is studied via Jeans' equation where effects of mass cascade are explicitly considered. The cascade induced radial flow tends to enhance the random motion in the outer region. Mass cascade leads to a nonzero halo surface energy/tension that are formulated explicitly. An effective exponent of gravitational interaction  $n_e = -1.3$  is obtained for virial theorem that is different from -1 due to halo surface energy. A stochastic model is proposed for the evolution of halo size that follows geometric Brownian motion and log-normal distribution. The stochastic model for particle random motion in randomly evolving halos (Brownian with multiplicative noise) leads to Fokker-Planck equations for particle probability distribution. Solutions provide fundamental relations between particle distribution and radial and osmotic flow. Complete solutions of particle distribution as well as other relevant halo properties are presented based on a simple model of osmotic flow. The proposed model agrees with simulation for a wide range of halo group sizes. With reference pressure and density defined at halo center, equation of state is established for relative pressure and density ( $\Delta p_{hm} \propto (\Delta \rho_{hm})^{b_r}$ ). The pressure, density, and velocity dispersion at halo center are also presented. The core size  $x_c$  is obtained where Hubble flow is dominant. Simple closures are proposed for self-consistent halo density description.

Key Words: Dark Matter Halo, Cusp-core, Halo energy, Density Profile, Equation of State, Collisionless, Mass/Energy Cascade, Self-gravitating

## Contents

Nomenclature .....	4
1. Introduction .....	5
2. The simulation data .....	8
3. Effects of inverse mass cascade on halo properties .....	8
3.1 Halo density profiles .....	8
3.2 Effects of inverse mass cascade on halo deformation and radial flow.....	9
3.3 Effects of radial flow on halo density distribution.....	14
3.4. The limiting value of concentration $c$ and radial momentum and kinetic energy .....	23
3.5. Effects of radial flow on halo velocity dispersion .....	25
3.6. Effects of mass cascade on halo energies and surface tension.....	32
4. Stochastic models for halo size and particle distribution function.....	39
4.1. Stochastic model for halo size evolution .....	39
4.2. Stochastic model for particle distribution .....	43
4.3. Equation of state for relative pressure and density .....	56
4.4. Simple closures for self-consistent particle distribution .....	60
5. Conclusion .....	60

## **Nomenclature**

See Supplementary Information

## 1. Introduction

The self-gravitating collisionless fluid dynamics (SG-CFD) is the study of motion of collisionless matter under the influence of its own gravity. A typical example is the large-scale gravitational collapse of collisionless system [1]. The self-organization of self-gravitating collisionless matter leads to the formation and evolution of large-scale structures due to the gravitational instability. Highly localized and virialized halos are major manifestation of nonlinear gravitational collapse [2, 3] and the building blocks of large-scale structures.

By contrast, incompressible hydrodynamics also develops instability if Reynolds number is sufficiently high, where turbulence starts to initiate and develop. The “eddies”, building blocks of turbulence, are formed at different length scales and interacting with each other, as described by a famous poem :“Big whirls have little whirls, That feed on their velocity; And little whirls have lesser whirls, And so on to viscosity” [4]. Large eddies feed smaller eddies, which feed even smaller eddies, and then lead to viscous dissipation at the smallest scale, i.e. the concept of a direct energy cascade. While direct energy cascade is the key feature of three-dimensional turbulence, two-dimensional turbulence possesses a range of scales over which kinetic energy is transferred from small to large scales , i.e. an inverse energy cascade [5].

The similarity between “eddies” in turbulence and “halos” in self-gravitating collisionless flow (SG-CFD) allows a new poem by simply replacing “whirls” with “halos”. “Little halos have big halos, That feed on their mass; And big halos have greater halos, And so on to growth”. This picture describes the inverse mass cascade of SG-CFD. There exists a broad spectrum of halo size. Small halos are created, interacting, and merging with other halos. Halos pass their mass onto larger and larger halos, until halo mass growth becomes dominant over mass propagation.

While “eddy” is not a well-defined object in turbulence literature, “halo” are well-defined dynamical objects, whose abundance and internal structure have been extensively studied over several decades. The abundance of halos is described by a halo mass function, a fundamental quantity to model structure formation and evolution. The seminal Press-Schechter (PS) model [6, 7] allows one to predict the shape and evolution of mass function. This model relies on a threshold value of density contrast that can be analytically derived from the nonlinear collapse of a spherical top hat over-density [8, 9]. Further improvement was achieved by extending the PS formalism with the elliptical collapse model [10, 11].

The internal structure of halos is primarily described by the halo density profile, another important quantity for structure formation and evolution [12]. Structure of halos can be studied both analytically and numerically with  $N$ -body simulations [13, 14]. The spherical collapse model relates the assumed power-law density with the initial density fluctuations, which can be dependent on the effective index of the power spectrum from the linear theory. This simple similarity model leads to an isothermal density profile for virialized halos. However, high-resolution  $N$ -body simulations of structure formation have shown that the simulated halos have a density shallower than the isothermal profile at smaller radius and steeper at larger radius [15, 16]. Many effects might contribute to this deviation. The dynamics of halo mass accretion/cascade is one of the most critical effect that is absent, which renders the simple similarity model invalid.

By revisiting fundamental ideas of turbulence, the inverse mass cascade is mathematically formulated [17]. Mass cascade is local, two-way, and asymmetric in mass space. Halos inherit/pass their mass mostly from/to halos of similar size. The net mass transfer proceeds in a “bottom-up” fashion. Two distinct ranges can be identified for mass cascade, i.e. a propagation range with a scale-independent rate of mass transfer  $\varepsilon_m$  and a deposition range with cascaded mass consumed

to form and grow halos. A fundamental merging frequency  $f_0 \sim m_p^{(\lambda-1)} a^{-\tau_0}$  between two single mergers of elementary mass  $m_p$  can be identified, where  $a$  is the scale factor,  $m_p$  is the particle mass,  $\lambda$  and  $\tau_0$  are two key mass cascade parameters that may be dependent on the exact cosmology model. The waiting time  $\tau_g$  (halo lifespan) for halos to pass their mass to larger halos scales as  $\tau_g \sim m_h^{-\lambda} a^{\tau_0}$ . Consequently, the everlasting inverse mass cascade with a scale-independent mass transfer rate  $\varepsilon_m \sim a^{-\tau_0}$  in the propagation range is a distinct feature of the intermediate statistically steady state of SG-CFD. This requires continues mass generation at the smallest scale at the same rate as  $\varepsilon_m$  for mass propagation. The entire mass cascade was also formulated by random-walk in mass space [17]. This results in a heterogeneous diffusion model with position-dependent diffusivity, where mass function can be analytically derived without relying on a specific spherical or elliptical collapse model.

This paper focus on the effects of inverse mass cascade on halo energy, momentum, size, and internal structure. Especially, it is still not clear why halos that form in SG-CFD have nearly universal profiles. This paper attempts to shed some light by considering direct effects of mass cascade. We will demonstrate that the in-flow in the halo outer regions (due to mass accretion or cascade) and out-flow in the halo core region (the Hubble flow) lead to an extra length scale for density profile where the radial flow is at its maximum. A double-power-law density is a natural result with inner density dominated by the halo deformation rate and outer density controlled by halo growth. The limiting halo concentration for large halos is a result of vanishing linear moment. The effects of mass cascade on velocity dispersion and surface energy are explicitly discussed and presented. Stochastic models for halo size and particle motion are also discussed with equation of state for halos presented. The rest of the paper is organized as follows: Section 2 introduces the

simulation and numerical data, followed by the effects of mass cascade on halo properties in Section 3. Stochastic models for halo size and random-walk of collisionless particles in halos with a varying size are presented in Section 4 with complete solutions provided.

## 2. The simulation data

The numerical data for this work is publicly available and generated from  $N$ -body simulations carried out by the Virgo consortium. A comprehensive description of the simulation data can be found in [18, 19]. The same set of simulation data has been widely used in a number of different studies from clustering statistics [19] to the formation of halo clusters in large scale environments [20], and testing models for halo abundance and mass functions [10]. More details can be found in supplementary information.

## 3. Effects of inverse mass cascade on halo properties

### 3.1 Halo density profiles

The formation of halos is a complex, hierarchical, and nonlinear process. However, the radial density profile  $\rho_h(r)$  of halos can be robustly fitted by relatively simple functions from cosmological  $N$ -body simulations. This section briefly reviews the NFW profile [15], the Einasto profile [21] and the power-law density profile (see supplementary information).

Both NFW and Einasto profiles involve a halo concentration parameter  $c = r_h/r_s$ , where  $r_h$  and  $r_s$  are the halo size and scale radius. Simulations have shown that the concentration  $c = r_h/r_s$  can be dependent on both halo mass and redshift. The evolution of  $c$  depends very much on the mass accretion rate and the faster the halo grows, the slower  $c$  increases. A constant value of  $c$  is expected for large halos with extremely fast mass accretion and short lifespan, where  $c \approx 4$  was



estimated as a limiting value for large halos from  $N$ -body simulations [22, 23]. The inner structures of these halos are still being dynamically adjusted by the mass accretion.

Supplementary Fig. S1 plots the variation of shape parameter  $\alpha$  of an Einasto profile with the concentration  $c$  (of a NFW profile) by numerically solving Eq. (S13). The shape parameter  $\alpha$  decreases from 0.2 to 0.155 for concentration  $c$  varying from 4 to 10, i.e.  $\alpha$  increases with increasing mass that is consistent with simulations [24].

### 3.2 Effects of inverse mass cascade on halo deformation and radial flow

Large halos with extremely short lifespan should have fast mass accretion rate. At the same redshift  $z$ , these halos are dynamical objects and should have a constant mean density regardless of their masses. The fast halo mass accretion with short lifespan during mass cascade affects the halo density profiles by creating a non-zero radial flow. To quantitatively formulate this idea, let's first consider the time variation of mass of these halos,

$$m_h(a) = \frac{4}{3} \pi r_h^3 \Delta_c \bar{\rho}_0 a^{-3}, \quad (1)$$

where  $\Delta_c = 18\pi^2$  is a critical density ratio that can be obtained from spherical collapse model.

Here  $\bar{\rho}_0$  is the background density at the current epoch of  $a = 1$ . The halo size  $r_h(a)$  is defined as the halo virial radius. Equation (1) implies that the circular velocity at the surface of halos satisfies (with  $H^2 a^3 = 8\pi G \bar{\rho}_0 / 3 = H_0^2$  for matter dominant model),

$$v_{cir}^2 = \frac{G m_h}{r_h} = 4\pi^2 \frac{r_h^2}{t^2} = (3\pi H r_h)^2, \quad (2)$$

where  $H(a)$  and  $H_0$  are the Hubble constants at scale factor  $a$  and the current epoch.

The following relation for the time variation of the halo size  $r_h$  with respect to the scale factor  $a$  can be obtained from Eq. (1),

$$\frac{\partial \ln r_h}{\partial \ln a} = \frac{1}{3} \frac{\partial \ln m_h}{\partial \ln a} + 1 = \frac{a}{3m_h} \frac{\partial m_h}{\partial a} + 1. \quad (3)$$

The time variation of typical halos of mass  $m_h$  can be expressed in terms of time scale  $\tau_g$ ,

$$\frac{\partial m_h}{\partial a} = \frac{1}{Ha} \frac{\partial m_h}{\partial t} = \frac{m_p}{\tau_g Ha}, \quad (4)$$

where  $\tau_g(m_h, a)$  is the mean waiting time (lifespan) of a given halo for merging with a single merger of mass  $m_p$  and passing its mass to large scale. After inserting Eq. (4) into Eq. (3),

$$\frac{\partial \ln r_h}{\partial \ln a} = \frac{m_p}{3\tau_g H m_h} + 1 = \frac{1}{3\tau_g H n_p} + 1, \quad (5)$$

where  $n_p = m_h/m_p$  is the number of particles in that halo. Next consider the halo density at the surface of halos (as shown in Fig. 1),

$$\rho_h(r=r_h) = \frac{N_s m_p}{4\pi r_h^2 r_p}, \quad (6)$$

where  $N_s$  is the number of elementary mass  $m_p$  within the spherical shell of the thickness  $r_p$ .

Figure 1 illustrates how the halo mass accretion changes the original halo size during an infinitesimal time interval  $dt$ . The original halo has a size  $r_h$  at time  $t$  (the dashed line). By the time  $t+dt$ , the halo size will increase from  $r_h$  to  $r_h - r_p' + r_p$  due to the mass accretion. The original halo surface (dashed line) shrinks to a smaller size of  $r_h - r_p'$  (solid line around green circle). First, halo mass accretion creates a new layer of mass around the original halo with a thickness of  $r_p - r_p'$ . Second, this layer of mass deforms the original halo (dark blue) to a new size

(green) due to the gravitational interaction. This deformation creates a non-zero inward radial flow of mass. For isothermal profile,  $r_p' = 0$  such that mass accretion does not deform the original halo.

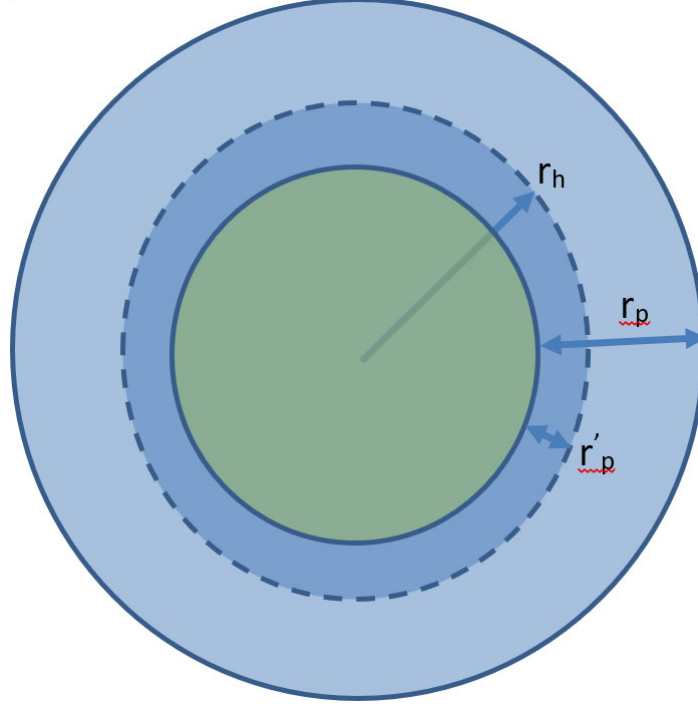


Figure 1. Schematic plot of halo mass accretion and size change during an infinitesimal time interval  $dt$ . Original halo has a size  $r_h$  at time  $t$  (the dash line in the plot). By the time  $t + dt$ , the halo size will increase from  $r_h$  to  $r_h - r_p' + r_p$  due to the mass accretion. The original halo at time  $t$  deforms to the new size of  $r_h - r_p'$  (green). Halo mass accretion/cascade creates a new layer of mass around the original halo with a thickness of  $r_p$ . This layer of mass potentially deforms the original halo to a new size (green) due to the gravitational interaction, which creates a non-zero radial flow of mass. Special case  $r_p' = 0$  (no radial flow) leads to an isothermal density profile.

The time variation of halo radius  $r_h$  due to mass accretion can be expressed as (with Eq. (6)),

$$\frac{\partial r_h}{\partial a} = \frac{1}{Ha} \frac{\partial r_h}{\partial t} = \frac{r_p - r_p'}{N_s \tau_g Ha} = \frac{m_p}{\tau_g Ha} \frac{1}{4\pi r_h^2 \rho_h(r_h)} \left( 1 - \frac{r_p'}{r_p} \right), \quad (7)$$

where  $N_s \tau_g$  is the total time it takes to form the new layer of mass. Equivalently, we have

$$\frac{\partial \ln r_h}{\partial \ln a} = \frac{m_p}{4\pi r_h^3} \frac{\alpha_h}{\tau_g H \rho_h(r_h)}, \quad (8)$$

where the incremental change in halo size is  $dr_h = r_p - r_p' = \alpha_h r_p$ . The halo deformation parameter

$\alpha_h = 1 - r_p'/r_p$  is introduced to reflect the effect of mass accretion on the halo deformation. The

mass density at the halo surface can be obtained by comparing Eq. (8) with Eq. (5),

$$\rho_h(r_h) = \frac{m_h}{4\pi r_h^3} \frac{3\alpha_h}{1 + 3\tau_g H n_p}. \quad (9)$$

From inverse mass cascade (Eq. (51) in ([17])), we can estimate that on average,

$$\tau_f(m_h^L, a) = \frac{1 - \lambda}{1 - 2\tau_0/3} t \sim t, \quad (10)$$

where the time scale  $\tau_f = \tau_g n_p$  is the time it takes to form the entire halo. Therefore,

$$\tau_g H n_p = \tau_f H = \frac{2(1 - \lambda)}{3 - 2\tau_0}. \quad (11)$$

With the help of Eq. (11), Eqs. (4) and (5) give the time variation of halo mass and halo size,

$$\frac{\partial \ln m_h}{\partial \ln a} = \frac{3 - 2\tau_0}{2(1 - \lambda)} \quad \text{and} \quad \frac{\partial \ln r_h}{\partial \ln a} = \frac{9 - 2\tau_0 - 6\lambda}{6(1 - \lambda)}, \quad (12)$$

both of which are dependent on two mass cascade parameters  $\lambda$  and  $\tau_0$ . Now, the time variation

of power-law density profile can be derived with Eqs. (S6) and (12),

$$\frac{\partial \ln \rho_h(r)}{\partial \ln a} = -3 + \frac{m(9 - 2\tau_0 - 6\lambda)}{6(1 - \lambda)}. \quad (13)$$

By comparing Eq. (9) with the power-law density profile in Eq. (S7), it is found that large halos should have a density profile of  $m = 3 - \alpha_h$  if parameters  $\lambda = 2/3$  and  $\tau_0 = 1$ . For an isothermal profile with  $m = 2$ , it is necessary that  $\alpha_h = 1$  or  $r_p' = 0$  such that mass accretion will not affect

the halo internal structure. The other limit is that  $\alpha_h = 0$  or  $r_p' = r_p$  (halo size gained from mass accretion exactly cancels the decrease in halo size due to the deformation) such that  $m = 3$  which is the maximum exponent for a power-law halo density profile.

We have the scaling laws of  $m_h \sim a^{3/2} \sim t$ ,  $r_h \sim a^{3/2} \sim t$ ,  $\rho_h(r=r_h) \sim r_h^{-2} \sim a^{-3}$ , and  $\rho_h(r) \sim a^0$  from Eqs. (12) and (13) for an isothermal profile. The halo density  $\rho_h(r)$  is time-invariant as a result of  $\alpha_h = 1$  such that the halo density at any radius  $r$  is fully determined at the moment that shell of halo is formed and will not change thereafter (Eq. (13)). This is the key feature of a power-law density profile that is different from NFW and Einasto profiles.

By comparing the density at the surface of halo (Eq. (9)) with the NFW density in Eq. (S5), the halo concentration parameter  $c$  can be related to the deformation parameter  $\alpha_h$ ,

$$\frac{\bar{\rho}_h(a)}{\rho_h(r_h, a)} = 3 \left[ \ln(1+c) - \frac{c}{1+c} \right] \left( 1 + \frac{1}{c} \right)^2 = \frac{1}{\alpha_h} \left( \frac{9 - 2\tau_0 - 6\lambda}{3 - 2\tau_0} \right). \quad (14)$$

The concentration parameter  $c$  is closely dependent on the halo deformation via  $\alpha_h$  and on the mass cascade via parameters  $\tau_0$  and  $\lambda$ . For large halos with  $c = 4$ , and parameters  $\lambda = 2/3$  and  $\tau_0 = 1$ , the deformation parameter  $\alpha_h \approx 0.79$ . For small halos with  $c = 10$  and mass cascade parameter  $\lambda = 2/3$  and  $\tau_0 = 1$ ,  $\alpha_h \approx 0.56$ . It is expected that the deformation parameter  $\alpha_h$  increases with the halo mass (smaller halos have relatively greater deformation and smaller  $\alpha_h$ ). The concentration-mass relation (the mass dependence of  $c$ ) might be related to the mass dependence of both  $\alpha_h$  and geometry parameter  $\lambda$  that should explore further.

### 3.3 Effects of radial flow on halo density distribution

The inverse mass cascade creates a new layer of mass that deforms the original halo to a new size (green in Fig. 1). This creates a non-zero radial flow that can be analyzed using the continuity equation. Let's start from a general self-similar expression of mass  $m_r(r, a)$ ,

$$m_r(r, a) = m_h(a) \frac{F(x)}{F(c)} \quad \text{and} \quad x(r, a) = \frac{r}{r_s(a)} = \frac{cr}{r_h(a)}, \quad (15)$$

where  $m_r(r, a)$  is the mass in a sphere of radius  $r$ ,  $x(r, a)$  is a reduced spatial-temporal variable that lumps the position  $r$  and scale factor  $a$  into a single variable. This general expression can represent both NFW (Eq. (S4)) and Einasto (Eq. (S10)), or any other density profiles via function  $F(x)$ . In principle, function  $F(x)$  can be an arbitrary unknown function that satisfies  $F(0) = 0$ . For example,  $F(x) = x$  for an isothermal profile. Equations (S3) and (S10) give expressions of  $F(x)$  for NFW and Einasto profiles. The halo density, potential, and velocity dispersion can all be determined in terms of unknown function  $F(x)$ . The halo density profile reads

$$\rho_h(r, a) = \frac{1}{4\pi r^2} \frac{\partial m_r(r, a)}{\partial r} = \frac{m_h(a)}{4\pi r_h^3} \frac{c^3 F'(x)}{x^2 F(c)}, \quad (16)$$

and the logarithmic slope of the halo density reads

$$\frac{\partial \ln \rho_h}{\partial \ln x} = \frac{\partial \ln F'(x)}{\partial \ln x} - 2 = x \frac{F''(x)}{F'(x)} - 2. \quad (17)$$

Evidently, the halo deformation parameter satisfies  $\alpha_h = cF'(c)/F(c)$  by comparing the density at halo surface to Eq. (9) with  $\lambda = 2/3$  and  $\tau_0 = 1$ . The time variation of function  $\rho_h(r, a)$  can be obtained from Eq. (16),

$$\frac{\partial \rho_h(r, a)}{\partial t} = \frac{1}{4\pi r^2} \frac{\partial^2 m_r(r, a)}{\partial r \partial t}. \quad (18)$$

The mass continuity equation for a spherical halo in spherical coordinate simply reads,

$$\frac{\partial \rho_h(r, a)}{\partial t} + \frac{1}{r^2} \frac{\partial [r^2 \rho_h(r, a) u_r(r, a)]}{\partial r} = 0, \quad (19)$$

where  $u_r(r, a)$  is the mean radial flow velocity. From Eqs. (18) and (19), the mass  $m_r(r, a)$  is related to the radial flow velocity as,

$$\frac{\partial m_r(r, a)}{\partial t} = -4\pi r^2 u_r(r, a) \rho_h(r, a). \quad (20)$$

With  $m_r(r, a)$  from Eq. (15) and  $\rho_h(r, a)$  from Eq. (16), the radial flow velocity reads

$$u_r(r, a) = -\frac{1}{4\pi r^2} \frac{\partial \ln m_r}{\partial \ln t} \frac{m_r(r, a)}{\rho_h(r, a)t} = -\frac{r_s(t)}{t} \frac{\partial \ln m_r}{\partial \ln t} \frac{F(x)}{F'(x)}. \quad (21)$$

While from Eq. (15) for  $m_r(r, a)$ , we have

$$\frac{\partial \ln m_r}{\partial \ln t} = \frac{\partial \ln m_h}{\partial \ln t} - \frac{x F'(x)}{F(x)} \frac{\partial \ln r_s}{\partial \ln t} - \frac{c F'(c)}{F(c)} \frac{\partial \ln c}{\partial \ln t}. \quad (22)$$

Substituting Eqs. (22) into (21), the radial flow has a very simple expression,

$$u_r(r, a) = \left[ x \frac{\partial \ln r_s}{\partial \ln t} + \left( \frac{\partial \ln F(c)}{\partial \ln t} - \frac{\partial \ln m_h}{\partial \ln t} \right) \frac{F(x)}{F'(x)} \right] \frac{r_s}{t}, \quad (23)$$

which is a general equation for mean radial flow with a time-varying concentration  $c$ . For small halos with a stable core and extremely slow mass accretion ( $\partial r_s / \partial t \approx 0$  and  $\partial m_h / \partial t \approx 0$ ) and constant  $m_r(r_s, a)$ , we shall expect that  $F(c) \propto m_h$  is almost a constant (from Eq. (15)) and  $u_r(r, a) = 0$  (Eq. (23)) that is consistent with the stable clustering hypothesis (small halos are virialized and well bound structures).

For the other limiting situation, i.e. large halos with extremely fast mass accretion and an expanding core, the concentration  $c$  is relatively a constant. Equation (23) reduces to

$$u_r(r, a) = \frac{1}{c} \left[ x - \frac{\partial \ln m_h}{\partial \ln r_h} \frac{F(x)}{F'(x)} \right] \frac{\partial r_h}{\partial t}. \quad (24)$$

In principle, the non-zero halo growth rate  $\partial r_h / \partial t$  should lead to a non-zero mean radial flow. A special case is the isothermal profile with  $F(x) = x$  and  $m_h \propto r_h$ , where  $u_r(r, a) = 0$ , i.e. a vanishing radial flow for isothermal profile even if  $\partial r_h / \partial t \neq 0$ . The radial flow  $u_r(r, a)$  is a function of reduced position  $x$  only and scaled by the rate of halo growth  $\partial r_h / \partial t$ . We introduce a dimensionless radial flow velocity  $u_h(x)$  (normalized by the core expanding speed  $r_s / t$ ) as

$$u_h(x) = \frac{cu_r(r, a)t}{r_h} = \frac{u_r(r, a)}{r_s/t} = \left[ \underbrace{x}_1 - \underbrace{\frac{\partial \ln m_h}{\partial \ln r_h} \frac{F(x)}{F'(x)}}_2 \right] \frac{\partial \ln r_h}{\partial \ln t}. \quad (25)$$

Clearly, the halo growth rate  $\partial r_h / \partial t$  affects the mean radial flow in Eq. (25). For large halos with a constant value of  $c$ ,  $\partial r_h / \partial t = r_h / t = v_{\text{cir}} / (2\pi)$  (Eq. (2)) does not varying with time and  $u_r(r, a)$  is self-similar and only dependent on the reduced variable  $x$ . The total radial flow can be decomposed into two contributions: 1) the outward flow due to the halo growth where  $u_r(r, a) = r/t$  (term 1), and 2) the inward flow due to the halo deformation (term 2).

By comparing the density at surface of halos (Eqs. (16) and (9)) and using the help of Eqs. (11) and (12), the constraints and boundary conditions of the radial flow velocity are,

$$u_h(x=0) = 0, \quad u_h(x=c) = c \left( 1 - \frac{1}{\alpha_h} \right) \frac{\partial \ln r_h}{\partial \ln t}, \quad \text{and} \quad x_0 = \frac{\partial \ln m_h}{\partial \ln r_h} \frac{F(x)}{F'(x)} \bigg|_{x=x_0}, \quad (26)$$



where  $u_h(x_0) = 0$ . Figure 2 plots the normalized radial velocity  $u_h(x)$  for three different density profiles. The NFW and Einasto profiles (for  $c = 4$  and  $\alpha = 0.2$ ) lead to a very similar radial flow velocity with out-flow ( $u_h(x) > 0$ ) for core region ( $x < x_0$ ) and in-flow ( $u_h(x) < 0$ ) for the outer region ( $x > x_0$ ) of halos, where  $u_h(x_0) = 0$ . The maximum radial flow is at  $x = 1$  or  $r = r_s$ . The total mass  $m_r(x, a)$  decreases with time for  $x < x_0$  and increases with time for  $x > x_0$  (from Eq. (20)). The difference between two profiles is that  $u_h(x \rightarrow 0) = x/2$  for NFW profile and  $u_h(x \rightarrow 0) = 2x/3$  for Einasto profile.

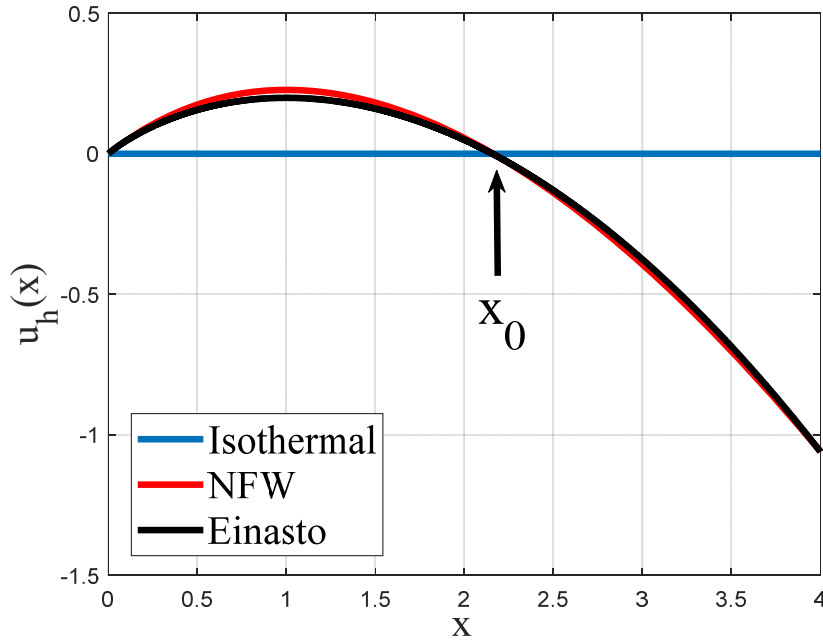


Figure 2. The normalized mean radial flow  $u_h(x)$  (Eq. (25)) for three different density profiles. The isothermal halo density corresponds to a vanishing radial flow. The NFW and Einasto profiles ( $c = 4$  and  $\alpha = 0.2$ ) lead to very similar radial flow with out-flow ( $u_h(x) > 0$ ) for the core region and in-flow ( $u_h(x) < 0$ ) for the outer region. The maximum radial flow is at  $x = 1$  or  $r = r_s$ . The mass  $m_r(r, a)$  inside the radius  $r$  decreases with time for  $x < x_0$  and increases with time for  $x > x_0$  (Eq. (20)). The circular velocity is at its maximum at  $x = x_0$ . The difference between two profiles is that  $u_h(x \rightarrow 0) = x/2$  for NFW and  $u_h(x \rightarrow 0) = 2x/3$  for Einasto profile.

The dimensionless peculiar radial flow can be obtained by subtracting the Hubble flow,

$$u_p(x) = u_h(x) - \frac{2}{3}x = \frac{1}{3}x - \frac{F(x)}{F'(x)}. \quad (27)$$

Especially for an isothermal profile with  $F(x) = x$ ,  $u_p(x) = -2x/3$ , which can be a good approximation of peculiar radial flow. This is consistent with the stable clustering hypothesis, i.e. the peculiar radial flow

$$u_p(x) \frac{r_s}{t} = -\frac{2}{3}x \frac{r_h}{ct} = -\frac{2}{3} \frac{cr}{r_h} \cdot \frac{r_h}{ct} = -Hr. \quad (28)$$

An interesting quantity is the angle  $\theta_{vr}$  between particle peculiar velocity (sum of peculiar radial velocity and circular velocity) and its position vector from the halo center of mass,

$$\cot(\theta_{vr}) = \frac{u_p(x)}{v_c(r, a)} \frac{r_h}{ct} = \frac{x}{2\pi c} \left( \frac{1}{3} - \frac{1}{\alpha_h} \cdot \frac{F'(c)}{F'(x)} \cdot \frac{cF(x)}{xF(c)} \right) \sqrt{\frac{xF(c)}{cF(x)}}, \quad (29)$$

where the circular velocity (normalized) at any radius  $r$  of the halo is

$$v_{nc}^2(r, a) = \frac{v_c^2(r, a)}{v_{cir}^2} = \frac{Gm_r(r, a)}{rv_{cir}^2} = \frac{cF(x)}{F(c)x}. \quad (30)$$

Interestingly,  $v_{nc}^2(x, a)$  is at its maximum when  $x = x_0$  where  $u_h(x_0) = 0$ . The quantity  $\cot(\theta_{vr})$  quantifies the ratio of radial motion (radial momentum) to the circular motion (angular momentum). With  $\alpha_h = cF'(c)/F(c)$ , the  $\cot(\theta_{vr})$  at the halo surface ( $x = c$ ) and at halo center ( $x = 0$ ) are obtained from Eq. (29) as

$$\cot(\theta_{vr}(x = c)) = \frac{1}{2\pi} \left( \frac{1}{3} - \frac{1}{\alpha_h} \right) \quad (31)$$

and

$$\cot(\theta_{vr}(x=0)) = \lim_{x \rightarrow 0} \frac{1}{2\pi c} \left( \frac{1}{3} - \frac{F(x)}{xF'(x)} \right) \sqrt{\frac{x^3 F(c)}{cF(x)}}. \quad (32)$$

When  $x = c$  at halo surface,  $\cot(\theta_{vr}) = -1/(3\pi)$  and  $\theta_{vr} \approx 96.06^\circ$  for  $\alpha_h = 1$  (isothermal profile) and  $\theta_{vr} \approx 98.44^\circ$  for  $\alpha_h = 0.79$  (NFW profile with  $c=4$  from Eq. (14)). From Eq. (32), the angle  $\theta_{vr}$  should gradually decrease to  $\theta_{vr} = 90^\circ$  ( $\cot(\theta_{vr}) = 0$  with  $u_p(x) \rightarrow 0$ ) at the core region for any  $F(x) \propto x^m$  ( $m \leq 3$ ) with  $x \rightarrow 0$ . This can be also demonstrated by a two-body gravitational collapse (TBCM) model.

By taking the derivative of  $u_h(x)$  (Eq. (25)) with respect to the reduced variable  $x$ ,

$$\frac{\partial u_h(x)}{\partial x} = \left[ 1 - \frac{\partial \ln m_h}{\partial \ln r_h} + \frac{\partial \ln m_h}{\partial \ln r_h} \frac{F(x)F''(x)}{F'^2(x)} \right] \frac{\partial \ln r_h}{\partial \ln t}. \quad (33)$$

Particularly for a NFW profile,

$$\frac{\partial u_h(x)}{\partial x} = \left[ \ln(1+x) - \frac{x}{1+x} \right] \frac{1-x^2}{x^2}. \quad (34)$$

It can be verified that for both NFW and Einasto profiles, the conditions of maximum flow ( $\partial u_h(x)/\partial x|_{x=1} = 0$ ) and logarithmic slope of -2 ( $\partial \ln \rho_h / \partial \ln x|_{x=1} = -2$ ) at scale radius ( $x = 1$  or  $r = r_s$ ) requires  $F''(x)|_{x=1} = 0$  (Eq. (17)). Hence,  $\partial \ln m_h / \partial \ln r_h = 1$  from Eq. (33), which further confirms that  $\tau_0 = 3\lambda/2$  for large halos (from Eq. (12)).

The existence of an extra length scale  $r_s$  origins from mass cascade induced radial flow. The in-flow at the halo outer region and the out-flow at the inner region creates a maximum mass flow rate at the scale radius  $r_s$  (or  $x = 1$ ) and introduces an extra length scale  $r_s$  for halo density profile, which does not exist for a scale-free isothermal density profile (Fig. 2).

We are especially interested in the logarithmic slope of the unknown function  $F'(x)$  that directly impacts the halo density profile (Eq. (16)). It can be obtained from the mean radial flow  $u_h(x)$  using Eqs. (25) and (33),

$$\frac{\partial \ln F'(x)}{\partial \ln x} = \frac{\frac{\partial u_h(x)}{\partial x} - \frac{\partial \ln r_h}{\partial \ln t} + \frac{\partial \ln m_h}{\partial \ln t}}{\frac{\partial \ln r_h}{\partial \ln t} - \frac{u_h(x)}{x}}. \quad (35)$$

Specially, for matter dominant system, we expect,

$$\frac{\partial \ln r_h}{\partial \ln t} = \frac{\partial \ln m_h}{\partial \ln t} = 1 \quad \text{and} \quad \frac{\partial \ln F'(x)}{\partial \ln x} = \frac{x F''(x)}{F'(x)} = \frac{\partial u_h / \partial x}{1 - u_h/x}. \quad (36)$$

The logarithmic slope of halo density profile (from Eq. (17)) reads

$$\frac{\partial \ln \rho_h}{\partial \ln x} = \frac{\partial \ln F'(x)}{\partial \ln x} - 2 = \frac{\partial u_h / \partial x}{1 - u_h/x} - 2. \quad (37)$$

We have simple expressions for NFW and Einasto profiles, respectively,

$$\frac{\partial \ln F'(x)}{\partial \ln x} = \frac{1-x}{1+x} \quad \text{and} \quad \frac{\partial \ln F'(x)}{\partial \ln x} = 2 - 2x^\alpha. \quad (38)$$

To provide some insights into the long-standing cusp-core controversy (core/cusp problem), a double-power-law density profile can be proposed as a natural result of Eq. (37). The inner halo density is determined by the velocity gradient (the halo deformation rate)  $\gamma_h = \partial u_h / \partial x|_{x=0}$  such that the inner halo density follows a power-law

$$\rho_h(r < r_s) \propto r^{(3\gamma_h - 2)/(1 - \gamma_h)} \quad (39)$$

that is dependent on parameter  $\gamma_h$  only. The smaller  $\gamma_h$  (slower deformation at the halo center) leads to a steeper density profile. Especially, for a matter dominant universe, the radial flow should be exactly the Hubble flow if both gravitational and pressure forces are not present in halos. If the

potential and pressure are symmetric functions of  $r$  and regular at origin  $r=0$ , the gravitational and pressure forces should vanish at origin such that  $u_r(r \rightarrow 0) = Hr$ . We expect the initial velocity of mass shells at the center of halo is simply the Hubble flow for halos with fast mass accretion,

$$u_r(r \rightarrow 0) = u_h(x \rightarrow 0) \frac{r_s}{t} = \gamma_h x \frac{r_s}{t} = \gamma_h \frac{r}{t} = Hr, \quad (40)$$

such that  $\gamma_h = Ht = 2/3$ . This means a central core with  $\rho_h(r < r_s) \propto r^0$  from Eq. (39) does exist for large halos with fast mass accretion.

For outer halo region (especially  $r \gg x_0$  in Fig. 2), we can approximate (using Eq. (26))

$$\frac{\partial u_h}{\partial x} \approx \frac{c(1-1/\alpha_h)}{c-x_0} \quad \text{and} \quad 1 - \frac{u_h}{x} \Big|_{x=c} \approx \frac{1}{\alpha_h}, \quad (41)$$

Such that from Eq. (37)

$$\rho_h(r > r_s) \propto r^{\frac{c(\alpha_h-1)}{c-x_0}-2}, \quad (42)$$

with a power-law density profile steeper than the isothermal profile of -2 for the outer halo region. Equations (39) and (42) provide a double-power-law density with inner density controlled by halo deformation rate parameter  $\gamma_h$  and outer density controlled by the halo growth via a halo deformation parameter  $\alpha_h$  and concentration  $c$ .

In principle, accurate halo density profiles can be obtained if the normalized mean flow  $u_h(x)$  is known. Without loss of generality, the Taylor expansion of  $u_h(x)$  around the center (up to the third order) can be given by

$$u_h(x) = a_0 + \gamma_h x + a_2 x^2 + a_3 x^3, \quad (43)$$

with three unknown coefficients. To satisfy the boundary conditions (26) and the constraint

$u_h(0) = 0$  and  $\partial u_h / \partial x|_{x=1} = 0$ , we have  $a_2$  and  $a_3$  expressed as

$$a_0 = 0, \quad a_2 = -\frac{(c^2 - 3)\gamma_h + 3 - 3/\alpha_h}{2c^2 - 3c}, \quad a_3 = \frac{(c - 2)\gamma_h + 2 - 2/\alpha_h}{2c^2 - 3c}. \quad (44)$$

The unknown function  $F(x)$  can be analytically solved from Eq. (25) and we have the solution,

$$F(x) = \exp \left\{ \frac{a_2/(\gamma_h - 1)}{\sqrt{4a_3(\gamma_h - 1) - a_2^2}} a \tan \left[ \frac{a_2 + 2a_3x}{\sqrt{4a_3(\gamma_h - 1) - a_2^2}} \right] \right\} \left( \frac{x^3}{x - u_h(x)} \right)^{\frac{1}{2(1-\gamma_h)}}, \quad (45)$$

with which the density profile can be obtained from Eq. (16).

We have shown that a complete description of  $u_h(x)$  or  $F(x)$  requires at least three parameters, the deformation rate parameter  $\gamma_h$  at the center of halo, the halo deformation parameter  $\alpha_h$  at the surface of halo, and the concentration  $c$  for the size of halos. The location  $x_0$  where  $u_h(x_0) = 0$  is estimated to be (from Eq. (43))

$$x_0 = \frac{-a_2 - \sqrt{a_2^2 - 4a_3\gamma_h}}{2a_3}, \quad (46)$$

with limiting values

$$x_0 = \frac{3}{2} \text{ for } \gamma_h \rightarrow 0 \quad \text{and} \quad x_0 = \frac{2c-3}{c-2} \text{ for } \gamma_h \rightarrow \infty. \quad (47)$$

The radial flow at  $x = 1$  and its derivative at  $x = c$  are,

$$u_h(x=1) = \frac{(c-1)^2 \gamma_h - (1-1/\alpha_h)}{c(2c-3)} \quad \text{and} \quad \left. \frac{\partial u_h}{\partial x} \right|_{x=c} = \frac{(c-3)\gamma_h + 6(1-1/\alpha_h)}{(2c-3)/(c-1)}. \quad (48)$$

An even simpler case is a Taylor expansion of  $u_h(x)$  up to the second order (i.e.  $a_3 = 0$ ) that will lead to solutions,

$$a_0 = 0, \quad a_2 = -\gamma_h/2, \quad \text{and} \quad \gamma_h = (1-1/\alpha_h)/(1-c/2) \quad (49)$$

from Eq. (44). We have  $x_0 = 2$  from Eq. (43) for expansion of  $u_h(x)$  up to the second order.

Alternatively, function  $F(x)$  might be modelled directly with the following constraints:

$$F(0)=0, F(x \rightarrow 0)=x^{1/(1-\gamma_h)}, \frac{cF'(c)}{F(c)}=\alpha_h, \text{ and } \left. \frac{\partial^2 F}{\partial x^2} \right|_{x=1}=0. \quad (50)$$

Solutions of all relevant quantities can be easily obtained with either  $u_h(x)$  or  $F(x)$  explicitly modelled. Therefore, the halo density profile can be found by the correct modeling of either the dimensionless radial flow  $u_h(x)$  or unknown function  $F(x)$ .

In short, the logarithmic slope of the density profile is continuously dependent on the mean radial flow  $u_h(x)$  (Eq. (37)). An accurate model of  $u_h(x)$  considering the effect of mass cascade can improve halo density models. Since the matter density spectrum is closely related to halo density profiles and mass functions, effects of mass cascade and accretion on the density spectrum can be further investigated.

### 3.4. The limiting value of concentration $c$ and radial momentum and kinetic energy

The limiting value of the concentration  $c \approx 4$  for large halos with fast mass accretion was estimated from  $N$ -body simulations. It is possible to analytically derive this limiting value by requiring a vanishing radial momentum for large halos with fast mass accretion. With Eq. (24) for mean flow  $u_r(r, a)$  and Eq. (16) for density  $\rho_h(r, a)$ , the radial linear momentum is

$$L_{hr}(a) = \int_0^{r_h} u_r(r, a) 4\pi r^2 \rho_h(r, a) dr = \frac{m_h v_{cir}}{2\pi c F(c)} \left( cF(c) - 2 \int_0^c F(x) dx \right). \quad (51)$$

With the unknown function  $F(x) = \ln(1+x) - x/(1+x)$  (Eq. S3) for NFW profile, the radial linear momentum reduces to

$$L_{hr}(a) = \frac{m_h v_{cir}}{2\pi c F(c)} \left( \frac{c(4+3c)}{1+c} - (4+c) \ln(1+c) \right). \quad (52)$$

The critical value of  $c$  for individual halos can be identified from the condition of a vanishing linear momentum (like spherical shells at turn-around point with a zero velocity in spherical collapse model). Therefore, by requiring  $L_{hr}(a) = 0$ , Eq. (51) becomes

$$cF(c) = 2 \int_0^c F(x) dx, \quad (53)$$

where it was found that  $c = 3.48$  for a NFW profile with  $F(x) = \ln(1+x) - x/(1+x)$ . With sufficiently fast mass accretion rate, halos keep growing with a vanishing radial momentum  $L_{hr}$ . For halos with  $c > 3.48$ , this self-similar solution leads to a negative radial linear momentum  $L_{hr} < 0$  indicating an overall in-flow of momentum. Next, the radial kinetic energy is given by,

$$\begin{aligned} K_{hr}(a) &= \frac{1}{2} \int_0^{r_h} u_r^2(r, a) 4\pi r^2 \rho_h(r, a) dr \\ &= \frac{m_h v_{cir}^2}{8\pi^2 c^2 F(c)} \left( c^2 F(c) - 4 \int_0^c x F(x) dx + \int_0^c \frac{F^2(x)}{F'(x)} dx \right). \end{aligned} \quad (54)$$

Specifically, the radial kinetic energy for a NFW profile is given by the expression of,

$$\begin{aligned} K_{hr} &= \frac{m_h v_{cir}^2}{8\pi^2 c^2 F(c)} \left[ 2 \ln(1+c) (5 - 10c - 5c^2 + (3 + 4c + c^2 + 2 \ln(-c)) \ln(1+c)) + \right. \\ &\quad \left. \frac{c(13c^2 + 7c - 10)}{(1+c)} + 8 \ln(1+c) \text{Polylog}(2, 1+c) - 8 \text{Polylog}(3, 1+c) + 8 \text{Zeta}(3) \right], \end{aligned} \quad (55)$$

which involves polylogarithm and zeta functions. In general, we can express both the radial linear momentum and radial kinetic energy in terms of the circular velocity  $v_{cir}$  (Eq. (2)) with two coefficients that are functions of  $c$ ,

$$L_{hr}(a) = \lambda_{Lr}(c) m_h v_{cir} \quad \text{and} \quad K_{hr} = \lambda_{Kr}(c) m_h v_{cir}^2. \quad (56)$$



With  $c = 3.48$  for NFW profile, we have  $\lambda_{Lr} = 0$  and  $\lambda_{Kr} = 7 \times 10^{-5}$ . Figure 3 plots the variation of two coefficients with the concentration  $c$ . Note that  $\lambda_{Kr}$  is rescaled by 100 times to be plotted in the same plot as  $\lambda_{Lr}$ . Halos with  $c > 3.48$  have increasing kinetic energy with  $c$ . Large halos with fast mass accretion have a vanishing radial linear momentum with  $c = 3.48$  and a (almost) minimum radial kinetic energy for all different concentration  $c$ . Large halos with fast mass accretion tend to grow with vanishing radial momentum and minimum radial kinetic energy.

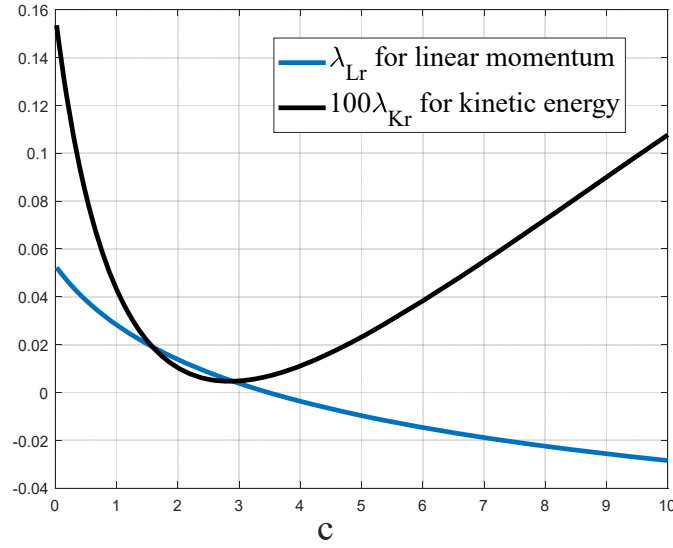


Figure 3. The variation of normalized radial momentum  $\lambda_{Lr}$  and kinetic energy  $\lambda_{Kr}$  with the concentration parameter  $c$  for a NFW profile. A limiting value of  $c = 3.48$  can be found for large halos with  $\lambda_{Lr} = 0$ , where the linear radial momentum vanishes. The normalized radial kinetic energy is also close to its minimum at the limiting value of  $c$ .

### 3.5. Effects of radial flow on halo velocity dispersion

The Jeans' equation coupled with the inverse mass cascade can be used to study the effect of radial flow on the velocity dispersion. First, the gravitational potential in terms of the unknown function  $F(x)$  reads

$$\phi_h(r, a) = -G \int_r^\infty \frac{m_r(y, a)}{y^2} dy = -v_{cir}^2 \frac{c}{F(c)} \int_x^\infty \frac{F(y)}{y^2} dy. \quad (57)$$

A shifted gravitation potential can be introduced to satisfy  $\phi_h^*(r=0, a) = 0$ ,

$$\phi_h^*(r, a) = \phi_h(r, a) + v_{cir}^2 \frac{c}{F(c)} \int_0^\infty \frac{F(y)}{y^2} dy = v_{cir}^2 \frac{c}{F(c)} \int_0^x \frac{F(y)}{y^2} dy. \quad (58)$$

The full dynamic Jeans' equation along the radial direction is usually written as

$$\underbrace{\frac{\partial u_r}{\partial t} + u_r \frac{\partial u_r}{\partial r}}_1 + \frac{1}{\rho_h} \frac{\partial (\rho_h \sigma_r^2)}{\partial r} + \frac{2}{r} \beta_h \sigma_r^2(r, a) = -\frac{\partial \phi_h(r, a)}{\partial r} = -\frac{Gm_r(r, a)}{r^2}, \quad (59)$$

where  $\sigma_r^2(r, a)$  is the radial velocity dispersion. The anisotropy of velocity dispersion is defined through an anisotropy parameter  $\beta_h = 1 - \sigma_t^2 / \sigma_r^2$ , where  $\sigma_t^2(r, a)$  is the tangential velocity dispersion. For isotropic velocity dispersion, we have  $\sigma_t = \sigma_r$  and  $\beta_h = 0$ . The full dynamic Jeans' equation (59) describes the evolution of non-zero radial flow for a non-rotating spherical halo if the halo velocity dispersion  $\sigma_r^2$  is known. The dynamics of a rotating halo with finite angular momentum is much more completed and will be presented in a separate paper.

Term 1 from the radial flow is often neglected for small virialized halos ( $u_r = 0$ ) and the radial velocity dispersion can be solved by the static Jeans equation with known  $m_r(r, a)$  or a given density profile [25]. However, large halos with fast mass accretion are dynamic objects, where mass cascade/accretion leads to a non-zero mean radial flow  $u_r$  that will contribute significantly to velocity dispersion (especially to the outer region of halos). Here we attempt to solve an inverse problem, i.e. solving for the velocity dispersion  $\sigma_r^2$  with a known mean radial flow  $u_r$ . After

substituting the expressions for  $m_r(r, a)$  (Eq. (15)) and  $u_r(r, a)$  (Eq. (24)) into Jeans' equation

(59) with the chain rule from  $x = r/r_s(t)$ ,

$$\frac{\partial}{\partial t} = \frac{\partial}{\partial x} \frac{\partial x}{\partial t} = -\frac{x}{t} \frac{\partial \ln r_s}{\partial \ln t} \frac{\partial}{\partial x} \quad \text{and} \quad \frac{\partial}{\partial r} = \frac{\partial}{\partial x} \frac{\partial x}{\partial r} = \frac{1}{r_s} \frac{\partial}{\partial x}, \quad (60)$$

The original Jeans' equation becomes

$$\underbrace{\sigma_r^2 \frac{\partial \ln(\rho_h \sigma_r^2)}{\partial \ln x}}_1 = x \underbrace{\frac{r_s^2}{t^2} \left[ \frac{\partial u_h}{\partial x} \left( x \frac{\partial \ln r_s}{\partial \ln t} - u_h \right) + u_h \left( 1 - \frac{\partial \ln r_s}{\partial \ln t} \right) \right]}_2 - \underbrace{v_c^2}_3. \quad (61)$$

An equivalent equation in terms of the function  $F(x)$  (using Eq. (16) for density) reads

$$\frac{c^2}{x \rho_h v_{cir}^2} \frac{\partial \rho_h \sigma_r^2}{\partial x} = \frac{1}{4\pi^2} \frac{F(x)^2 F''(x)}{x F'(x)^3} - \frac{\rho_h(x)}{\bar{\rho}_h(a)} \frac{3F(x)}{x F'(x)}, \quad (62)$$

where  $v_c$  is the circular velocity at radius  $r$  (Eq. (30)) and  $\bar{\rho}_h(a)$  is the average halo density. Here, the  $\partial \ln r_s / \partial \ln t = 1$  from mass cascade was used (Eq. (12)). Three terms in equation. Term 1 comes from the pressure gradient due to the radial velocity dispersion, term 2 is due to the nonzero radial flow, and term3 comes from gravity.

For small halos with a stable core, the stable clustering hypothesis is valid and  $u_h = 0$  (term 2 vanishes), where the pressure (term 1) exactly balances the gravity (term 3) everywhere. While for the other limiting situation, i.e. large halos with fast mass accretion, the Hubble flow ( $u_h(x) = 2x/3$ ) at halo center leads to a central core with a finite core density  $\rho_h(0) \equiv \rho_h(x=0)$ .

For core region with  $u_h(x) = 2x/3$ , Eq. (62) can be transformed to

$$\frac{c^2}{x \rho_h(x) v_{cir}^2} \frac{\partial(\rho_h \sigma_r^2)}{\partial x} = \frac{1}{\Delta_c} - \frac{\rho_h(x)}{\bar{\rho}_h(a)} = -\delta(x) \frac{\bar{\rho}(a)}{\bar{\rho}_h(a)}, \quad (63)$$

where  $\Delta_c = 18\pi^2$  is the critical density ratio,  $\delta(x)$  is the overdensity at location  $x$ . The pressure in the core region can be approximated by a parabolic function of  $x$  (from Eq. (63)),

$$p_h(x) = \rho_h(x) \sigma_r^2(x) = p_h(x=0) - \frac{1}{2} J_c x^2, \quad (64)$$

where the constant  $J_c$  in the unit of pressure is obtained from Eq. (63),

$$J_c = \left( \frac{\rho_h(0)}{\bar{\rho}_h} - \frac{1}{18\pi^2} \right) \frac{\rho_h(0) v_{cir}^2}{c^2} \approx \frac{\rho_h^2(0) v_{cir}^2}{\bar{\rho}_h c^2}. \quad (65)$$

A core size  $x_c$  where Hubble flow is dominant can be defined by setting  $p_h(x_c) = 0$  in Eq. (64),

$$x_c = \sqrt{\frac{2\bar{\rho}_h(a)}{\rho_h(0)}} \frac{c\sigma_r(0)}{v_{cir}}. \quad (66)$$

Next, let's work on the velocity dispersion profile. The general expression for the radial dispersion  $\sigma_r^2$  reads (from Eq. (62))

$$\frac{\partial}{\partial x} \left[ \frac{F'(x) \sigma_r^2}{x^2} \right] = \frac{F'(x)}{x^2} \frac{r_s^2}{t^2} \left[ \frac{\partial u_h}{\partial x} \left( x \frac{\partial \ln r_s}{\partial \ln t} - u_h \right) + u_h \left( 1 - \frac{\partial \ln r_s}{\partial \ln t} \right) \right] - \frac{Gm_h}{r_h} \frac{cF(x)F'(x)}{F(c)x^4}. \quad (67)$$

If we applies the evolution of halo size  $r_h \sim t$  or  $\partial \ln r_h / \partial \ln t = 1$  due to the mass accretion, the integration of Eq. (67) leads to an explicit expression for radial dispersion normalized by the circular velocity  $\sigma_{nr} = \sigma_r / v_{cir} = \sigma_r t / (2\pi r_h)$  (with help from Eqs. (2) and (33)),

$$\sigma_{nr}^2 = \underbrace{\frac{x^2}{4\pi^2 c^2 F'(x)} \left\{ \frac{F^2(x)}{x^2 F'(x)} \Big|_x^\infty - \int_x^\infty \left[ \frac{2F(x)}{x^2} - \frac{2F^2(x)}{F'(x)x^3} \right] dx \right\}}_1 + \underbrace{\frac{cx^2}{F'(x)} \int_x^\infty \frac{F(x)F'(x)}{F(c)x^4} dx}_2,$$

or equivalently,

$$\sigma_{nr}^2 = \underbrace{\frac{x^2}{4\pi^2 c^2 F'(x)} \int_x^\infty \frac{F(x)^2}{x^2} \left( \frac{1}{F'(x)} \right)' dx}_1 + \underbrace{\frac{cx^2}{F'(x)} \int_x^\infty \frac{F(x)F'(x)}{F(c)x^4} dx}_2 \quad (68)$$

with two separate contributions from radial flow (term 1) and from gravitational potential (term 2), respectively. Term 1 is usually neglected for small virialized halos with  $u_r = 0$ , but can be important for large halos with fast mass accretion. Here we require the pressure term  $(\rho_h \sigma_r^2)|_{x=\infty} = 0$  at infinity when integrating Eq. (67).

For an isothermal profile with  $F(x) = x$ , the normalized dispersion has a constant value of  $\sigma_{nr}^2 = 1/2$ . For NFW profile with  $F(x) = \log(1+x) - x/(1+x)$ , two contributions can be derived explicitly from Eq. (68). Term 1 reads

$$\sigma_{nr1}^2 = -\frac{(1+x)^2}{36\pi^2 x^2 c^2} \left\{ 3x^2 - 4\pi^2 x^3 + 12x^3 \text{poly log}(2, 1+x) - \right. \\ \left. \left[ 3(1+x)^2 (2x-1) \ln(1+x) + 6x - 12x^2 - 12x^3 \ln x - 12i\pi x^3 \right] \ln(1+x) \right\}, \quad (69)$$

with an approximation of  $\sigma_{nr1}^2 \approx \left( \frac{1}{18} - \frac{1}{3\pi^2} \right) \frac{x}{c^2}$  for  $x \rightarrow 0$ . Term 2 becomes

$$\sigma_{nr2}^2 = \frac{c \ln(1+x)}{2xF(c)} + \frac{c}{2F(c)} \left\{ -1 - 9x - 7x^2 + \left[ -2 - 8x - 4x^2 + x^3 \right] \ln(1+x) + \right. \\ \left. \left[ \pi^2 + 6 \text{poly log}(2, -x) - \ln x + 3(\ln(1+x))^2 \right] x(1+x)^2 \right\}, \quad (70)$$

with the approximation  $\sigma_{nr2}^2 \approx -\frac{c}{2F(c)} x \ln(x)$  for  $x \rightarrow 0$ . Figure 4 plots the variation of the total radial velocity dispersion  $\sigma_{nr}^2(x) = \sigma_{nr1}^2(x) + \sigma_{nr2}^2(x)$  for an isothermal profile and NFW profile ( $c = 4$ ). The two separate contributions are also presented in the same plot, i.e.  $\sigma_{nr1}^2(x)$  from the mean radial flow and  $\sigma_{nr2}^2(x)$  from the gravitational potential, respectively. The first contribution from mean radial flow tends to enhance the radial velocity dispersion and is only significant at a large  $x$  for the outer region of a halo.

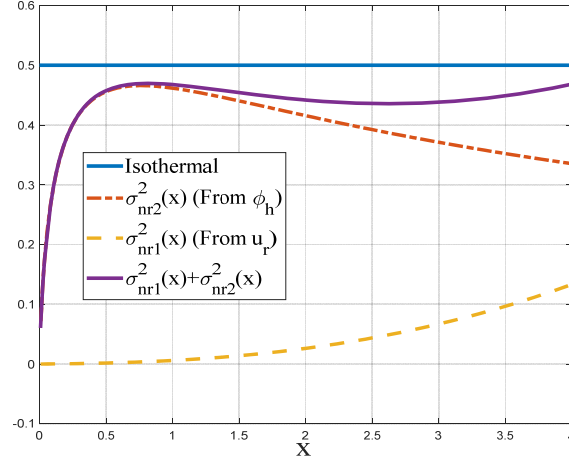


Figure 4. The normalized radial velocity dispersion  $\sigma_{nr}^2(x)$  for an isothermal profile (a constant value of  $1/2$ ) and NFW profile (varying with  $x$  for  $c = 4$ ) with two contributions, i.e.  $\sigma_{r1}^2(x)$  from the mean radial flow (Eq. (69)) and  $\sigma_{r2}^2(x)$  from the gravitational potential (Eq. (70)), respectively. The radial flow tends to enhance the radial random motion and is only significant for large  $x$  in the halo outer region.

Now we have complete solutions of radial pressure and potential for halos with a NFW profile with effect of radial flow or mass cascade was included. Both are normalized by the circular velocity  $v_{cir}$  and read (with the help of Eq. (16) for density and Eq. (57) for potential)

$$p_{nr}(x) = \frac{\rho_h \sigma_r^2}{\bar{\rho}_h v_{cir}^2} = \frac{c^3 F'(x)}{3F(c)x^2} \sigma_{nr}^2(x), \quad (71)$$

$$\phi_{nh}(x) = \frac{\phi_h}{v_{cir}^2} = -\frac{c \ln(1+x)}{xF(c)}. \quad (72)$$

Supplementary Fig. S2 plots the normalized pressure  $p_{nr}(x)$  (Eq. (71)), gravitational potential

$\phi_{nh}(x)$  (Eq. (72) and radial velocity dispersion  $\sigma_{nr}^2(x)$  (Eqs. (68)) for a NFW profile with  $c = 4$ .

The halo density  $\rho_{nh}(x)$  is normalized by the halo mean density  $\bar{\rho}_h$ . The density

$\rho_{nh}(x \rightarrow 0) \sim x^{-1}$  and pressure  $p_{nr}(x \rightarrow 0) \sim -\log(x)$ . This leads to an Equation of State

$p_{nr}(x \rightarrow 0) \sim a + b \log(\rho_{nh})$  for NFW profile (Eq. (70)). Both pressure and density fields are divergent and irregular at the center of halo.

A convenient formula for the logarithmic slope of radial pressure can be derived from the full Jeans' equation (Eq. (62)) for  $\partial \ln r_h / \partial \ln t = 1$ , where

$$\frac{\partial \ln p_{nr}}{\partial \ln x} = \frac{x^2 - x u_h}{4\pi^2 c^2 \sigma_{nr}^2} \frac{\partial u_h}{\partial x} - \frac{v_{nc}^2}{\sigma_{nr}^2}. \quad (73)$$

Similarly, two contributions can be identified (from the mean radial flow  $u_h$  and gravitational potential, respectively). At the scale radius  $r_s$ ,  $\partial u_h / \partial x|_{x=1} = 0$  and the logarithmic slope is exactly  $-v_{nc}^2 / \sigma_{nr}^2$ . The slope equals -2 everywhere for an isothermal profile.

With expressions for all relevant halo quantities explicitly derived, the scaling of these quantities in core region is summarized in Table 1 that is fully determined by the deformation rate parameter  $\gamma_h$ . It should be noted that the circular velocity and velocity dispersion follows same scaling ( $v_c^2(r) \sim \phi_h^*(r) \sim \sigma_r^2(r)$ ) if  $\gamma_h < 1/2$ , regardless of the exact value of  $\gamma_h$ .

Table 1. Scaling around center of halo for different deformation rate parameter  $\gamma_h$

	$y$	Isotherm al	NFW	Einasto	Loose core	Dense core
$\gamma_h \geq 0$		$\gamma_h = 0$	$\gamma_h = 1/2$	$\gamma_h = 2/3$	$2/3 < \gamma_h < 1$	$\gamma_h > 1$
$F(x) \propto x^y$ (Eq. (50))	$y = \frac{1}{1 - \gamma_h}$	$y = 1$	$y = 2$	$y = 3$	$y > 3$	$y < 0$
$u_h(x) \propto \gamma_h x^y$ (Eq. (25))	$y = 1$	$y = 1$	$y = 1$	$y = 1$	$y = 1$	$y = 1$
$v_c^2(x) \propto x^y$ (Eq. (30))	$y = \frac{\gamma_h}{1 - \gamma_h}$	$y = 0$	$y = 1$	$y = 2$	$y > 2$	$y < 0$
$\rho_h(x) \propto x^y$ (Eq. (16))	$y = \frac{3\gamma_h - 2}{1 - \gamma_h}$	$y = -2$	$y = -1$	$y = 0$	$y > 0$	$y < -3$

$\phi_h^*(x) \propto x^y$ (Eq. (58))	$y = \frac{\gamma_h}{1-\gamma_h}$	diverge at $r = 0$	$y = 1$	$y = 2$	$y > 2$	$y < 0$
$\sigma_r^2(x) \propto x^y$ (Eq. (68))	$\frac{1}{2} < \gamma_h < \frac{2}{3}$ $y = \frac{2-3\gamma_h}{1-\gamma_h}$	N/A	N/A	$y = 0$	$y = 2$	N/A
	$\gamma_h = 1/2$	N/A	$-x \ln(x)$	N/A	N/A	N/A
	$\gamma_h < \frac{1}{2}$ $y = \frac{\gamma_h}{1-\gamma_h}$	$y = 0$	N/A	N/A	N/A	N/A

### 3.6. Effects of mass cascade on halo energies and surface tension

For completeness in studying the effects of mass cascade on halo properties, the (total) energies of entire halos are studied in this section. It was found that contributions from the radial flow to velocity dispersion could be important and should not be neglected for large halos. In contrast to small halos, large halos with fast mass accretion are dynamic objects with an expanding size, which should impact halo energies. Multiplying the continuity Eq. (19) by the mean radial flow  $u_r$  and the Jeans' equation (59) by density  $\rho_h$ , and adding two equations together, we have the equation

$$\frac{\partial(\rho_h u_r)}{\partial t} + \frac{1}{r^2} \frac{\partial(\rho_h r^2 u_r^2)}{\partial r} + \frac{\partial(\rho_h \sigma_r^2)}{\partial r} + \rho_h \frac{Gm_r(r, a)}{r^2} = 0. \quad (74)$$

Multiplying Eq. (74) by  $4\pi r^3$  and integrating with respect to  $r$  from 0 to  $r_h$  leads to an exact energy equation for non-rotating halos ,

$$I_h + S_u + S_\sigma - 2K_u - 6K_\sigma - \Phi_h = 0, \quad (75)$$

with all terms here normalized by  $m_h v_{cir}^2$ . This is a generalized version of virial theorem, as the standard virial theorem does not include the contributions from a nonzero radial flow (the surface energy  $S_u$  and the kinetic energy  $K_u$ ). Since  $r_h = r_h(t)$ , the integration of the first term in Eq. (74) can be separated into two contributions using the Leibniz's rule,



$$\int_0^{r_h} 4\pi r^3 \frac{\partial(\rho_h u_r)}{\partial t} dr = \frac{\partial G_h}{\partial t} - 4\pi r_h^3 \rho_h(r_h) u_r(r_h) \frac{\partial r_h}{\partial t}, \quad (76)$$

where a halo virial quantity

$$G_h = \int_0^{r_h} 4\pi r^3 \rho_h u_r dr = \frac{m_h(t) v_{cir}^2 t}{4\pi^2 c^2 F(c)} \left[ c^2 F(c) - 3 \int_0^c x F(x) dx \right] \quad (77)$$

is defined as the first order moment of radial flow. The virial quantity for peculiar velocity that excludes the Hubble flow reads

$$G_{hp} = \int_0^{r_h} 4\pi r^3 \rho_h (u_r - Hr) dr = \frac{m_h(t) v_{cir}^2 t}{4\pi^2 c^2 F(c)} \left[ \frac{1}{3} c^2 F(c) - \frac{5}{3} \int_0^c x F(x) dx \right]. \quad (78)$$

For comparison,  $L_{hr}(a)$  is the (zeroth order) linear momentum of radial flow. The (normalized) time derivative of the virial quantity ( $I_h$ ) is obtained as,

$$I_h = \frac{1}{m_h v_{cir}^2} \frac{\partial G_h}{\partial t} = \left[ \frac{1}{2\pi^2} - \frac{3}{2\pi^2 c^2 F(c)} \int_0^c x F(x) dx \right]. \quad (79)$$

The surface energy terms include the contribution  $S_u$  from the surface pressure due to the radial flow at halo surface,

$$S_u = \frac{4\pi r_h^3 \rho_h(r_h)}{m_h v_{cir}^2} \left[ u_r^2(r_h) - u_r(r_h) \frac{\partial r_h}{\partial t} \right] = \frac{1}{4\pi^2} \left[ \frac{F(c)}{c F'(c)} - 1 \right] = \frac{1/\alpha_h - 1}{4\pi^2} \quad (80)$$

and the contribution  $S_\sigma$  from the surface pressure due to the velocity dispersion at halo surface.

Since the radial velocity dispersion has two contributions (Eq. (68)), we have two corresponding contributions to the pressure term  $S_\sigma$ , i.e. from the radial flow ( $S_{\sigma 1}$ ) and from the gravitational potential ( $S_{\sigma 2}$ ), respectively,

$$S_\sigma = \frac{4\pi r_h^3 \rho_h(r_h) \sigma_r^2(r_h)}{(m_h v_{cir}^2)} = S_{\sigma 1} + S_{\sigma 2}, \quad (81)$$

$$S_{\sigma_1} = \frac{c}{4\pi^2 F(c)} \int_c^\infty \frac{F^2(x)}{x^2} \left( \frac{1}{F'(x)} \right)' dx \quad (82)$$

or

$$S_{\sigma_1} = \frac{c}{4\pi^2 F(c)} \left\{ \left( \frac{F^2(x)}{x^2 F'(x)} \right) \Big|_c^\infty - \int_c^\infty \left[ \frac{2F(x)}{x^2} - \frac{2F^2(x)}{F'(x)x^3} \right] dx \right\}, \quad (83)$$

$$S_{\sigma_2} = \frac{c^4}{F^2(c)} \int_c^\infty \frac{F(x)F'(x)}{x^4} dx. \quad (84)$$

The total kinetic energy of a halo includes the contribution directly from radial flow,

$$K_u = \lambda_{Kr} = \frac{\int_0^{r_h} 4\pi r^2 \rho_h u_r^2 dr}{2m_h v_{cir}^2} = \frac{1}{8\pi^2} - \frac{\int_0^c xF(x) dx}{2\pi^2 c^2 F(c)} + \frac{1}{8\pi^2 c^2 F(c)} \int_0^c \frac{F^2(x)}{F'(x)} dx. \quad (85)$$

Similarly, the second contribution of kinetic energy is from velocity dispersion (random motion) that again includes contributions from radial flow ( $K_{\sigma_1}$ ) and from gravitational potential ( $K_{\sigma_2}$ ), respectively, according to Eq. (68),

$$K_\sigma = \frac{1}{2m_h v_{cir}^2} \int_0^{r_h} 4\pi r^2 \rho_h \sigma_r^2 dr = K_{\sigma_1} + K_{\sigma_2}, \quad (86)$$

$$K_{\sigma_1} = \frac{1}{8\pi^2 c^2 F(c)} \int_0^c x^2 \left[ \int_x^\infty \frac{F(y)^2}{y^2} \left( \frac{1}{F'(y)} \right)' dy \right] dx \quad (87)$$

or if  $\lim_{x \rightarrow \infty} F(x)^2 / x^2 F'(x) = 0$ ,

$$K_{\sigma_1} = -\frac{1}{24\pi^2 c^2 F(c)} \left\{ \int_0^c \left( \frac{F(x)}{F'(x)} + 2x \right) F(x) dx + c^3 \int_c^\infty \left[ \frac{2F(x)}{x^2} - \frac{2F^2(x)}{F'(x)x^3} \right] dx \right\}. \quad (88)$$

The kinetic energy of velocity dispersion due to gravitational interaction is

$$K_{\sigma_2} = \frac{c^4}{6F^2(c)} \int_c^\infty \frac{F(x)F'(x)}{x^4} dx + \frac{c}{6F^2(c)} \int_0^c \frac{F(x)F'(x)}{x} dx. \quad (89)$$

The total gravitational potential of a halo is given by,

$$\Phi_h = -\frac{1}{m_h v_{cir}^2} \int_0^{r_h} 4\pi r^2 \rho_h \frac{Gm_r}{r} dr = -\frac{c}{F^2(c)} \int_0^c \frac{F(x)F'(x)}{x} dx. \quad (90)$$

In principle, we can derive the explicit expressions for all these terms for a halo with a known function of  $F(x)$ . For example, some of these terms for a NFW profile are presented here,

$$I_h = \frac{[5c^2 + 6c - 2(1+c)(c+3)\log(1+c)](c-3)}{8\pi^2 c^2 (1+c) [\log(1+c) - c/(1+c)]}, \quad (91)$$

$$S_u = \frac{[\log(1+c) - c/(1+c)](1+c)^2 - c^2}{4\pi^2 c^2}, \quad (92)$$

$$\Phi_h = -\frac{c[c(2+c) - 2(1+c)\ln(1+c)]}{2[\ln(1+c) - c/(1+c)]^2 (1+c)^2}. \quad (93)$$

Figure 5 plots the variation of these energy terms with the concentration  $c$  for halos with a NFW profile. The dynamic term  $I_h(c)$  is positive for small  $c$  and negative for large  $c$  with a critical concentration around  $c = 3$  where  $I_h = 0$ . The surface energy  $S_u$  due to radial flow is negative for small  $c$  and changing to positive for large  $c$ . The total kinetic energy  $K_u + K_{\sigma_1}$  due to radial flow is small compared to the kinetic energy purely due to the velocity dispersion  $K_{\sigma_2}$ , while the total surface energy  $S_u + S_{\sigma_1}$  due radial flow is comparable to  $S_{\sigma_2}$  due to velocity dispersion and should not be neglected. This can be explained by the fact that the mean radial flow is only significant in the outer region of halos.

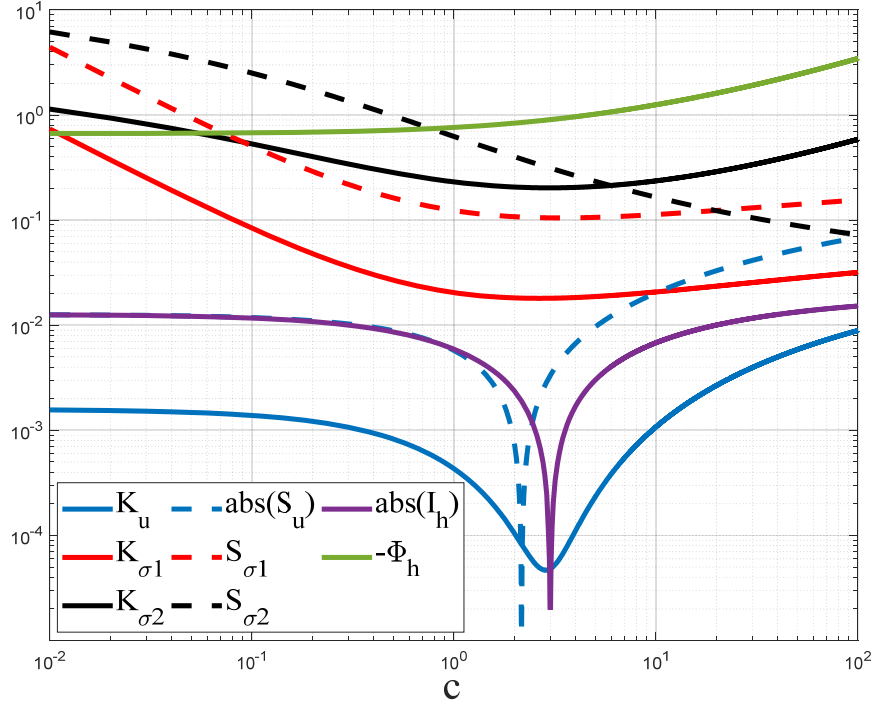


Figure 5. The log-log variation of various halo energies with the halo concentration parameter  $c$  for NFW profile. The dynamic term  $I_h(c)$  is positive for small  $c$  and negative for large  $c$ , while the surface energy  $S_u(c)$  due to radial flow is negative for small  $c$  and changing to positive for large  $c$ . The kinetic energy  $K_u + K_{\sigma1}$  due to the radial flow is small compared to the kinetic energy purely due to the velocity dispersion  $K_{\sigma2}$ , while the surface energy  $S_u + S_{\sigma1}$  is comparable to  $S_{\sigma2}$ . This can be explained by the fact that radial flow is only significant in outer region of halos.

Among these terms,  $I_h$  due to the mean radial flow is relatively small for large halos. The other three terms from radial flow should not be neglected and contribute to the total energy balance with  $S_{\sigma1} > K_{\sigma1} > S_u$ . By neglecting the dynamic term  $I_h$  and using Eq. (75), we may write the surface energy of large halos with fast mass accretion,

$$S_{eh} = (S_u + S_{\sigma1} + S_{\sigma2}) m_h v_{cir}^2 = \left[ 2(K_u + 3K_{\sigma2} + 3K_{\sigma1}) + \Phi_h \right] m_h v_{cir}^2, \quad (94)$$

which is the extra energy required to create the expanding halo surface. The halo surface energy is also the difference between the total energy of the halo with and without the halo surface. The equivalent halo surface tension can be introduced as the surface energy per unit area,

$$S_{th} = \frac{S_{eh}}{2A_h} = \frac{2(K_u + 3K_{\sigma 2} + 3K_{\sigma 1}) + \Phi_h}{8\pi r_h^2} m_h v_{cir}^2, \quad (95)$$

where  $A_h = 4\pi r_h^2$  is the surface area of a halo. For large halos with the limiting concentration  $c = 3.48$ , the normalized surface tension (from Eq. (95)) is estimated to be around

$$S_{nth} = \frac{2A_h S_{th}}{m_h v_{cir}^2} = \frac{S_{eh}}{m_h v_{cir}^2} \approx 0.3 \text{ for a NFW profile}$$

and

$$S_{nth} = \frac{2A_h S_{th}}{m_h v_{cir}^2} = \frac{S_{eh}}{m_h v_{cir}^2} = 0.5 \text{ for an isothermal profile.} \quad (96)$$

The normalized surface tension  $S_{nth}$  is a constant regardless of halo mass and time. An equation analog to the Young–Laplace equation can be written to relate the pressure difference across the halo surface to halo radius, or equivalently the halo surface curvature,

$$\Delta P_h = \frac{2S_{th}}{r_h} = \frac{S_{eh}}{A_h r_h} = \frac{1}{3} [S_u + S_{\sigma 1} + S_{\sigma 2}] \bar{\rho}_h v_{cir}^2 = \frac{1}{3} S_{nth} \bar{\rho}_h v_{cir}^2. \quad (97)$$

The pressure difference across the surface is  $\Delta P_h \approx 0.1 \bar{\rho}_h v_{cir}^2$ , which is approximately the pressure on halo surface. For a non-spherical halo, pressure may be different at different location depending on the local curvature.

We can introduce surface density for a given halo as  $\rho_{sur} = N_s m_p / A_h$ , where  $N_s$  is the number of particles on surface. Halo surface tension (an inherent property of halo surface) may be fully described by the surface density  $\rho_{sur}$ , gravitational constant  $G$ , and halo size  $r_h$ ,

$$S_{th} = \alpha_{st} (G)^{\alpha_1} (\rho_{sur})^{\alpha_2} (r_h)^{\alpha_3}, \quad (98)$$

where  $\alpha_{st}$  is a numerical constant. A simple dimensional analysis leads to expression

$$S_{th} = \alpha_{st} G \rho_{sur}^2 r_h, \quad (99)$$

where the halo surface density reads (after inserting Eq. (96) into (99))

$$\rho_{sur} = \sqrt{\frac{S_{nth}}{8\pi\alpha_{st}}} \frac{m_h}{r_h^2}. \quad (100)$$

For halos with  $\lambda = 2/3$  and  $\tau_0 = 1$ , we have  $m_h \propto r_h$ , the halo surface tension  $S_{th} \propto r_h^{-1}$ , the halo surface density  $\rho_{sur} \propto r_h^{-1}$  and the thickness of the halo surface layer  $r_p = \rho_{sur} / \rho_h(r_h) \propto r_h$  from Eq. (6). A complete list of dependence of these parameters on the mass cascade parameters  $\lambda$  and  $\tau_0$  is presented in Table 2.

Table 2. The dependence of power-law exponent  $m$  ( $\sim a^m$ ) on mass cascade

$m_h$	$r_h$	$\rho_{sur}$	$S_{th}$	$v_{cir}^2$	$r_p$
$\frac{3-2\tau_0}{2(1-\lambda)}$	$\frac{9-2\tau_0-6\lambda}{6(1-\lambda)}$	$\frac{12\lambda-9-2\tau_0}{6(1-\lambda)}$	$\frac{6\lambda-3-2\tau_0}{2(1-\lambda)}$	$\frac{3\lambda-2\tau_0}{3(1-\lambda)}$	$\frac{9-2\tau_0-6\lambda}{6(1-\lambda)}$
Eq. (12)	Eq. (12)	Eq. (100)	Eq. (95)	Eq. (2)	Eq. (6)

From Table 2, the thickness of surface layer  $r_p$  is proportional to halo size  $r_h$  ( $r_p \propto r_h$ ) regardless of the exact values of  $\lambda$  and  $\tau_0$  that may depend on the exact cosmology. This hints a geometric Brownian process (incremental change proportional to current value) for halo size in Section 5.1.

An effective exponent for gravitational interaction  $n_e$  can be introduced based on the virial theorem for halos with fast mass accretion and expanding size,

$$n_e = \frac{2(K_u + 3K_{\sigma 2} + 3K_{\sigma 1})}{\Phi_h} = \frac{S_{nth}}{\Phi_h} - 1. \quad (101)$$

With  $c = 3.48$  and  $\Phi_h \approx -1$ , the effective exponent  $n_e \approx -1.3$ . The deviation of  $n_e \approx -1.3$  from -1 (the actual potential exponent  $V(r) \approx r^{-1}$ ) reflects the dynamic effects of expanding size due to inverse mass cascade and mass accretion. This can be confirmed directly by N-body simulations.

#### 4. Stochastic models for halo size and particle distribution function

##### 4.1. Stochastic model for halo size evolution

The random walk of halos in mass space was applied to derive the halo mass functions [17]. Similarly, stochastic models can be developed for halo size and particle distributions that describe halo internal structure. The halo structure (the distribution of particles) is highly dependent on the evolution of halo size, and therefore on the mass cascade. In mass cascade, the halo waiting time  $\tau_{gr}$  is a random variable and follows an exponential distribution with mean  $\tau_g = \langle \tau_{gr} \rangle \propto m_h^{-\lambda}$ . The evolution of mass  $m_h$  of halos can be modeled by a stochastic process with perturbations due to the randomness in halo waiting time  $\tau_{gr}$ ,

$$\frac{\partial m_h}{\partial t} = \frac{m_p}{\tau_{gr}} = \frac{m_h}{\tau_g n_p^L} \cdot \frac{\tau_g m_h^L}{\tau_{gr} m_h}, \quad (102)$$

where  $m_h^L = \langle m_h \rangle$  is the mass of the typical halo if that halo always evolves with a deterministic waiting time  $\tau_g = \langle \tau_{gr} \rangle$ . Here  $n_p^L$  is the number of particles in  $m_h^L$ . Equation (102) becomes deterministic equation describes evolution of  $m_h^L$  by replacing the random waiting time  $\tau_{gr}$  with the mean waiting time  $\tau_g$ . By introducing the random variable

$$\xi_{gr}(t) = \frac{\tau_g m_h^L}{\tau_{gr} m_h} - 1 \quad \text{and} \quad \tau_g n_p^L = \frac{3(1-\lambda)}{3-2\tau_0} t \quad (\text{from Eq. (11)}), \quad (103)$$

we will have a stochastic differential equation for  $m_h$

$$\frac{\partial \ln m_h}{\partial \ln t} = \frac{3-2\tau_0}{3(1-\lambda)} (1 + \xi_{gr}(t)), \quad (104)$$

where  $\xi_{gr}$  is approximately a Gaussian random variable with zero mean. Equation (104) reduces to Eq. (12) for  $\xi_{gr} \rightarrow 0$ . As shown in Eqs. (4) and (8), the original equation for the evolution of mass and size of a typical halo can be generalized to stochastic models that read

$$\frac{\partial \ln m_h}{\partial \ln t} = \frac{m_p t}{m_h \tau_{gr}} \quad (105)$$

and

$$\frac{\partial \ln r_h}{\partial \ln t} = \frac{m_p}{4\pi r_h^3} \frac{\alpha_h t}{\tau_{gr} \rho_h(r_h)} = \frac{\alpha_h \bar{\rho}_h}{3\rho_h(r_h)} \frac{m_p t}{m_h \tau_{gr}} = \frac{\partial \ln m_h}{\partial \ln t} \frac{\alpha_h \bar{\rho}_h}{3\rho_h(r_h)}, \quad (106)$$

where the average waiting time  $\tau_g$  is simply replaced by a random waiting time  $\tau_{gr}$ . Finally, we have the stochastic equation for halo size from Eqs. (104) and (106),

$$\frac{\partial \ln r_h}{\partial \ln t} = \frac{\partial \ln m_h}{\partial \ln t} \frac{\alpha_h \bar{\rho}_h}{3\rho_h(r_h)} = \frac{3-2\tau_0}{3(1-\lambda)} \frac{\alpha_h \bar{\rho}_h}{3\rho_h(r_h)} (1 + \xi_{gr}(t)). \quad (107)$$

Halos evolving with a vanishing noise term in Eq. (107) always satisfy Eq. (1) with mean halo density  $\bar{\rho}_h = \Delta_c \bar{\rho}_0 a^{-3}$ . However, the existence of noise term  $\xi_{gr}$  in Eq. (107) may drive halos away from Eq. (1). At any instant of time  $t$ , we assume the relation (from Eqs. (106) and (12))

$$\frac{\partial \ln m_h}{\partial \ln r_h} = \frac{3\rho_h(r_h)}{\alpha_h \bar{\rho}_h} = \frac{3\rho_{sur}}{\alpha_h r_p \bar{\rho}_h} = \frac{3(3-2\tau_0)}{9-2\tau_0-6\lambda} \quad (108)$$



to be always valid, where  $\bar{\rho}_h(a)$  is the average halo density. This equation is required for both Eq. (104) and (107) to be valid simultaneously. Since  $\alpha_h \bar{\rho}_h \propto \rho_h(r_h)$ , the halo concentration  $c$  is also a constant of time from Eqs. (S5) or Eq. (S12). Therefore, these stochastic models describe randomly evolving mass and size of halos with constant concentration  $c$  (with fast mass accretion) and satisfying condition (108) at any instant  $t$ , i.e.  $m_h \propto r_h$  for  $\tau_0 = 1$  and  $\lambda = 2/3$ . The halos size  $r_h(t)$  should evolve as

$$\frac{dr_h}{dt} = b_{rh} \frac{r_h(t)}{t} (1 + \xi_{gr}(t)) \quad \text{with} \quad b_{rh} = \frac{9 - 2\tau_0 - 6\lambda}{9(1 - \lambda)} \quad (109)$$

from Eqs. (107) and (108), which is a geometric Brownian motion with a multiplicative noise. The parameter  $b_{rh}$  is from mass cascade and  $b_{rh} = 1$  for  $\tau_0 = 1$  and  $\lambda = 2/3$ .

The evolution of halo size can be also understood as a result of fluctuating halo surface with a random velocity proportional to the velocity dispersion at the halo surface, i.e. the radial velocity dispersion  $\sigma_r(r=r_h)$  discussed in Section 3. The stochastic differential equation with an initial halo size of  $r_h(t=t_i) = r_{h0}$  reads,

$$\frac{dr_h(t)}{dt} = b_{rh} \frac{r_h(t)}{t} + \beta_{rh} \sigma_r(r_h) \bar{\xi}_{rh}(t), \quad (110)$$

which is consistent with Eq. (109). The covariance of the noise term in term 2 satisfies

$$\langle \bar{\xi}_{rh}(t) \bar{\xi}_{rh}(t') \rangle = \delta(t - t') / H.$$

It is shown that the velocity dispersion at halo surface  $\sigma_r(r_h) = \alpha_{rh}(c) v_{cir} = 3\pi\alpha_{rh} H r_h$  from Eqs. (2), (69) and (70), where  $\alpha_{rh}(c)$  is a constant. For a limiting value of  $c \approx 3.48$ ,  $\alpha_{rh} = 1/\sqrt{2}$  for an isothermal profile. After transforming the physical time  $t$  to scale factor  $a$ , Eq. (110) reads

$$\frac{dr_h(t)}{dt} = \frac{3}{2} b_{rh} H r_h(t) + \underbrace{H r_h(t) \xi_{rh}(t)}_2, \quad (111)$$

and

$$\frac{dr_h(t)}{d \ln a} = \frac{3}{2} b_{rh} r_h(t) + r_h(t) \xi_{rh}(t), \quad (112)$$

where the multiplicative noise  $r_h(t) \xi_{rh}(t)$  (proportional to  $r_h$ ) describes the random evolution of halo size. The covariance of new noise  $\xi_{rh}(t)$  satisfies

$$\langle \xi_{rh}(t) \xi_{rh}(t') \rangle = 2 D_{rh} \delta(t - t') / H, \quad (113)$$

or equivalently the noise term  $\xi_{gr}(t)$  in Eq. (109) satisfies

$$\langle \xi_{gr}(t) \xi_{gr}(t') \rangle = 4 D_{rh} t \delta(t - t') / (3 b_{rh}^2), \quad (114)$$

where  $D_{rh} = (3\pi\alpha_{rh}\beta_{rh})^2/2$  is the diffusion coefficient.

The halo size  $r_h(t)$  described by the geometric Brownian motion (Eq. (112)) has a lognormal probability distribution of

$$P_{rh}(r_h, t) = \frac{1}{r_h \sqrt{8\pi D_{rh} \ln(t/t_i)/3}} \exp \left\{ -\frac{(\ln(r_h/r_{h0}) - (b_{rh} - 2D_{rh}/3) \ln(t/t_i))^2}{8D_{rh} \ln(t/t_i)/3} \right\}, \quad (115)$$

with the  $m$ th order moment of

$$\langle r_h^m \rangle = r_{h0}^m (t/t_i)^{mb_{rh} + \frac{2}{3}m(m-1)D_{rh}}. \quad (116)$$

The mean halo size grows linearly with time as  $\langle r_h(t) \rangle = r_{h0} (t/t_i)^{b_{rh}} \sim t^{b_{rh}}$ , as expected. The mode of the halo size grows as  $r_{h0} (t/t_i)^{b_{rh} - 2D_{rh}}$  and the median halo size grows as  $r_{h0} (t/t_i)^{b_{rh} - 2D_{rh}/3}$ .

Finally, the root mean square of halo size scales as  $\langle r_h^2 \rangle^{1/2} = r_{h0} (t/t_i)^{b_{rh} + 2D_{rh}/3}$ . Similarly, the halo mass ( $m_h \propto r_h$ ) will also follow a lognormal distribution.

#### 4.2. Stochastic model for particle distribution

To find the halo density profile, we need to derive the particle distribution function. The particle motion in halos is complicated as it is coupled to the varying halo size. Let's consider the motion of a collisionless particle in a halo with a stochastically varying size according to Eq. (111) and the goal is to derive the particle distribution function. The random position of that particle is

$$r_i(t) = x_i(t) r_s(t) = x_i(t) r_h(t) / c, \quad (117)$$

where  $r_h(t)$  is a stochastic time-varying halo size,  $x_i(t)$  is the reduced position of that particle to the center of halo. For halos with a fixed size,  $x_i(t)$  is expected to be a smooth function of time  $t$ . The time variation of particle position  $r_i(t)$  comes from both the time variation of  $x_i(t)$  and the variation of random halo size  $r_h(t)$ , i.e.  $cd r_i = x_i(t) dr_h + r_h(t) dx_i$ . The infinitesimal change  $dr_h$  is presented in stochastic Eq. (111). The infinitesimal change  $dx_i$  for a fixed  $r_h(t)$  is determined by the mean radial flow from Eq. (25),

$$u_h(x_i) = \underbrace{b_{rh} x_i - b_{rh} \frac{F(x_i)}{F'(x_i)}}_{\text{term 1}} \quad \text{with} \quad b_{rh} = \left\langle \frac{\partial \ln r_h}{\partial \ln t} \right\rangle \text{ (Eq. (109)).} \quad (118)$$

Here, term 1 is the particle motion relative to the halo size change. Therefore, the infinitesimal change  $dx_i$  for a fixed halo size  $r_h(t)$  can be written as

$$r_s(t) \frac{dx_{iF}}{dt} = \frac{r_s(t)}{t} \left[ u_h(x_i) - b_{rh} x_i + u_h^*(x_i) \right], \quad (119)$$

and

$$r_s(t) \frac{dx_{tB}}{dt} = \frac{r_s(t)}{t} \left[ u_h(x_t) - b_{rh} x_t - u_h^*(x_t) \right], \quad (120)$$

for forward and backward change of  $x_t(t)$  in time, respectively. Here  $u_h(x_t) - b_{rh} x_t$  is the radial flow relative to the halo size change. The current velocity  $u_h^*(x_t)$  turns out to be the osmotic flow velocity acquired by particles in equilibrium to the external force. In Einstein's theory of Brownian motion, it has an origin from the osmotic pressure. Applying chain rule to Eq. (117),

$$\frac{dr_t}{dt} = \frac{x_t(t)}{c} \frac{dr_h}{dt} + r_s(t) \frac{dx_t}{dt}$$

and inserting Eqs. (111) with  $r_s(t) = r_h(t)/c$  leads to the equation for particle position

$$\frac{dr_t}{dt} = \frac{r_s(t)}{t} \left[ t \frac{dx_t}{dt} + b_{rh} x_t \right] + x_t(t) r_s(t) H \xi_{rh}(t). \quad (121)$$

By inserting Eqs. (119) and (120) into Eq. (121), the stochastic equations for particle position  $r_t(t)$  for forward and backward processes reads,

$$\frac{dr_t}{dt} = \underbrace{\frac{r_s(t)}{t} \left[ u_h(x_t) + u_h^*(x_t) \right]}_1 + \underbrace{\sigma(x_t) r_s(t) H \xi_{rh}(t)}_2, \quad (122)$$

$$\frac{dr_t}{dt} = \underbrace{\frac{r_s(t)}{t} \left[ u_h(x_t) - u_h^*(x_t) \right]}_3 + \sigma(x_t) r_s(t) H \xi_{rh}^*(t). \quad (123)$$

The stochastic process  $r_t(t)$  is not differentiable with respect to time  $t$ , where the forward/backward velocities (the left/right side time derivatives of  $r_t(t)$ ) can be different. The mean radial flow  $u_h(x_t)$  (or the current velocity) is the average of forward (term 1) and backward (term 3) velocities, while the osmotic flow  $u_h^*(x_t)$  (or the fluctuation velocity) is the difference

between forward and backward velocities that changes its sign in terms 1 and 3. Both  $u_h(x_t)$  and  $u_h^*(x_t)$  contribute to the drift (terms 1 and 3) in Eqs. (122) and (123), while the mean drift at given  $x_t$  is the mean radial flow  $u_h(x_t)$ , as  $u_h^*(x_t)$  is cancelled out.

Noise terms  $\xi_{rh}(t)$  and  $\xi_{rh}^*(t)$  in term 2 represent the particle random motion due to a stochastic halo size  $r_h(t)$ , where  $\xi_{rh}(t)$  is independent of  $r_t(s)$  for  $s \leq t$  and  $\xi_{rh}^*(t)$  is independent of  $r_t(s)$  for  $s \geq t$ . The function  $\sigma(x_t)$  indicates that the noise is of a multiplicative nature, i.e. the noise is dependent on the process  $x_t$  itself. Here  $\sigma(x_t) = x_t$  is expected (see Eq. (121)) because the halo size follows a geometric Brownian motion (Eq. (111)).

By comparing with Eqs. (S15) and (S16) for regular Brownian motion in Supplementary Information, Eqs. (122) and (123) describe the random motion of collisionless particles with multiplicative noise because of halos varying in size due to mass cascade. This provides some fundamental insights into the halo internal structure. The corresponding Fokker-Planck equations (forward and backward in time) for the unique probability  $P_r(r, t) = P_r(x(t))$  of the particle position  $r_t$  are used to describe the forward and backward processes, respectively,

$$\frac{\partial P_r(r, t)}{\partial t} = -\frac{r_s(t)}{t} \frac{\partial}{\partial r} \left[ (u_h(x) + u_h^*(x)) P_r \right] + r_s^2(t) HD_{rh} \frac{\partial^2}{\partial r^2} (\sigma^2(x) P_r), \quad (124)$$

$$\frac{\partial P_r(r, t)}{\partial t} = -\frac{r_s(t)}{t} \frac{\partial}{\partial r} \left[ (u_h(x) - u_h^*(x)) P_r \right] - r_s^2(t) HD_{rh} \frac{\partial^2}{\partial r^2} (\sigma^2(x) P_r). \quad (125)$$

Applying the chain rule from Eq. (60) and adding/subtracting Eqs. (124) to/from Eq. (125) lead to two independent equations for velocities  $u_h(x)$  and  $u_h^*(x)$ ,

$$b_{rh} x \frac{\partial P_r}{\partial x} = \frac{\partial}{\partial x} [u_h(x) P_r], \quad (126)$$

$$u_h^*(x) = d_r \sigma^2(x) \frac{\partial}{\partial x} \ln[\sigma^2(x) P_r(x)], \quad (127)$$

where  $d_r = D_{rh} Ht = 2D_{rh}/3$ . The integration of continuity Eq. (126) leads to the same expression as we have derived for  $u_h(x)$  in Eq. (25). For comparison, the osmotic velocity of standard Brownian motion has a dimensional form of  $u_h^* = D \nabla \rho / \rho$  (i.e. related to the diffusion flux), where  $D$  is the diffusivity and  $\rho$  is the particle number density (See supplementary information Eq. (S14) for more details).

As demonstrated in Section 3.3 (Eqs. (43) to (45)), the radial number density function  $P_r(x)$  can be derived if the mean radial flow  $u_h(x)$  is known. Similarly, the number density  $P_r(x)$  can be easily found for a given osmotic flow  $u_h^*(x)$  and  $\sigma^2(x)$  from Eq. (127),

$$P_r(x) = \frac{\alpha_s}{\sigma^2(x)} \exp \left\{ \frac{1}{d_r} \int \frac{u_h^*(x)}{\sigma^2(x)} dx \right\}, \quad (128)$$

where  $\alpha_s$  is a normalization constant for probability  $P_r(x)$ . For isothermal profile with constant radial number density  $P_r(x)$ ,  $u_h(x) = 0$  and  $u_h^*(x) = d_r \partial \sigma^2(x) / \partial x$ .

For a given function of  $\sigma(x)$ , a key relation between two velocities (the mean radial and the osmotic flow) can be obtained from Eqs. (126) and (127),

$$u_h^*(x) = \frac{d_r \sigma^2(x)}{x - u_h(x)} \frac{\partial u_h}{\partial x} + d_r \frac{\partial \sigma^2(x)}{\partial x}. \quad (129)$$

The closure problem of halo density profile is now equivalent to find an additional relation between two velocities  $u_h^*(x)$  and  $u_h(x)$ . That relation combined with Eq. (129) will provide complete and consistent solutions of  $u_h(x)$  and  $u_h^*(x)$ . Solutions for all other the relevant halo quantities can

be obtained subsequently. Unlike the simple closure  $u_h = -u_h^*$  for Brownian motion, more work is required along this line to better understand the fundamental mechanism behind a universal halo structure. A simple closure is proposed and discussed in supplementary information.

For a NFW profile, we have (from Eqs. (126) and (127))

$$P_r(x) = \frac{x}{(1+x)^2}, \quad u_h(x) = 1 + 2x - \frac{(1+x)^2}{x} \ln(1+x), \quad \text{and} \quad u_h^*(x) = d_r \frac{x(3+x)}{1+x}, \quad (130)$$

where the integral of  $P_r(x)$  diverges, a well-known difficulty of NFW profile. At this time, we will take a different route to model the halo internal structure by first identifying basic properties of the osmotic flow  $u_h^*(x)$ . A simple model of  $u_h^*(x)$  is proposed, followed by applying Eq. (128) to derive the particle number density  $P_r(x)$ . Without loss of generality, let's assume a general power-law of  $\sigma(x) = x^{\lambda_r}$  (we expect  $\lambda_r = 1$  though) and from Eq. (127),

$$u_h^*(x) = d_r x^{2\lambda_r-1} \left( \frac{\partial \ln P_r}{\partial \ln x} + 2\lambda_r \right). \quad (131)$$

The derivative of  $u_h^*(x)$  is

$$\frac{\partial u_h^*(x)}{\partial x} = d_r x^{2\lambda_r-2} \frac{\partial^2 \ln P_r}{\partial (\ln x)^2} + (2\lambda_r - 1) \frac{u_h^*(x)}{x}. \quad (132)$$

The properties of  $u_h^*(x)$  can be identified from above equations,

$$u_h^*(x=0) = 0, \quad u_h^*(x=x_0^*) = 0 \quad \text{when} \quad \left. \frac{\partial \ln P_r}{\partial \ln x} \right|_{x=x_0^*} = \left. \frac{\partial \ln \rho_h}{\partial \ln x} \right|_{x=x_0^*} + 2 = -2\lambda_r, \quad (133)$$

and

$$u_h^*(x=1) = 2\lambda_r d_r \quad \text{because} \quad \left. \frac{\partial \ln P_r}{\partial \ln x} \right|_{x=1} = \left. \frac{\partial \ln \rho_h}{\partial \ln x} \right|_{x=1} + 2 = 0, \quad (134)$$

where  $x=1$  is the mode of probability function  $P_r(x)$ . Specifically, for  $\lambda_r = 1$  (From Eq. (129)),

$$\left. \frac{\partial u_h^*}{\partial x} \right|_{x=0} = \gamma_r = d_r \frac{2 - \gamma_h}{1 - \gamma_h}, \quad (135)$$

where  $\gamma_h = (\partial u_h / \partial x)|_{x=0}$  is the halo deformation parameter we defined before (Table 1).

Similar to the mean radial flow  $u_h(x)$ , the osmotic flow  $u_h^*(x)$  initially increases as  $\gamma_r x$  and reaches a maximum, then decreases to zero at  $x = x_0^*$  where the logarithmic slope of density  $\rho_h$  is  $-2 - 2\lambda_r$  (Eq. (133)). A simple and general model of  $u_h^*(x)$  (a simple expansion around  $x=0$ ) with three free parameters satisfying all conditions in (133), (134) and (135) can be written as,

$$u_h^*(x) = \gamma_r x - \beta_r x^{1+\alpha_r} \quad \text{with} \quad \alpha_r > 0. \quad (136)$$

Obviously the condition Eq. (134) requires,

$$\beta_r = d_r \left( \frac{2 - \gamma_h}{1 - \gamma_h} - 2\lambda_r \right). \quad (137)$$

The general solution of  $P_r(x)$  can be obtained from Eq. (128) with given  $u_h^*(x)$ ,

$$P_r(x) = \alpha_s x^{-2\lambda_r} \exp \left\{ \frac{x^{2-2\lambda_r}}{d_r} \left( \frac{\gamma_r}{2-2\lambda_r} - \frac{\beta_r x^{\alpha_r}}{2-2\lambda_r + \alpha_r} \right) \right\} \quad \text{for } \lambda_r \neq 1, \quad (138)$$

where  $\alpha_s$  is a normalization constant and

$$P_r(x) = \frac{\alpha_r x^{\gamma_r/d_r - 2}}{\Gamma[(\gamma_r - d_r)/(\alpha_r d_r)]} \left( \frac{\beta_r}{\alpha_r d_r} \right)^{\frac{\gamma_r - d_r}{\alpha_r d_r}} \exp \left\{ -\frac{\beta_r x^{\alpha_r}}{\alpha_r d_r} \right\} \quad \text{for } \lambda_r = 1. \quad (139)$$

The requirement of the maximum mean radial flow at  $r = r_s$  ( $\partial P_r / \partial x|_{x=1} = 0$  from Eq. (33)) means that the scale radius  $r_s$  or  $x=1$  is the mode of distributions  $P_r(x)$ , i.e. we will find maximum number of particles at  $r = r_s$ . For  $\partial P_r / \partial x|_{x=1} = 0$  applied to Eq. (138), we have the



relation  $2d_r\lambda_r = \gamma_r - \beta_r$ . Specifically, for  $\lambda_r = 1$ , relations between the drift and noise terms in Eqs. (122) and (123) are found as (analogy to the fluctuation-dissipation theorem)

$$2d_r = \gamma_r - \beta_r \quad \text{and} \quad \gamma_r = d_r \frac{2 - \gamma_h}{1 - \gamma_h}, \quad (140)$$

such that the particle distribution function (Eq. (139)) is reduced to a two-parameter distribution

$$P_r(x) = \frac{b_r^{a_r}}{\Gamma(a_r)(a_r - b_r)} \exp\left(-b_r x^{\frac{1}{a_r - b_r}}\right) x^{\frac{b_r}{a_r - b_r}} \quad (141)$$

in terms of two parameters  $a_r = (\gamma_r - d_r)/(\alpha_r d_r)$ ,  $b_r = \beta_r/(\alpha_r d_r)$ , and  $\alpha_r = 1/(a_r - b_r)$ .

If we require  $\gamma_r = \gamma_h$  for  $x \rightarrow 0$  (i.e. the inward particle motion  $u_h(x) - u_h^*(x)$  vanishes at the center of halo), we can determine that the constant  $d_r = 1/6$  (hence  $D_{rh} = 1/4$ ) with  $\gamma_h = 2/3$  from Eq. (40) that is required by Hubble flow at halo center. The other option is to require  $\gamma_r = 2\gamma_h$  for  $x \rightarrow 0$  (the inward particle motion  $u_h(x) - u_h^*(x) = -u_h(x)$ , i.e. the inward mass flow to the halo center balances the outward mass flow). The constant  $d_r = 1/3$  (hence  $D_{rh} = 1/2$ ). The values of relevant parameters for different options are listed in Table 3.

Table 3. Values of relevant parameters for three possible options

$\gamma_r$	$\gamma_h$	$D_{rh}$	$d_r$	$\lambda_r$	$\beta_r$	$a_r$	$b_r$	$u_h(x \rightarrow 0)$	$u_h^*(x \rightarrow 0)$
1/2	2/3	3/16	1/8	1	1/4	$3/\alpha_r$	$2/\alpha_r$	$2x/3$	$x/2$
2/3	2/3	1/4	1/6	1	1/3	$3/\alpha_r$	$2/\alpha_r$	$2x/3$	$2x/3$
4/3	2/3	1/2	1/3	1	2/3	$3/\alpha_r$	$2/\alpha_r$	$2x/3$	$4x/3$

The function  $F_r(x)$  is the fraction of particles with a distance smaller than a given  $x$ , i.e. the cumulative distribution function of the probability  $P_r(x)$ ,

$$F_r\left(x = \frac{r}{r_s}\right) = \int_0^x P_r(y) dy = \frac{m_r}{m_h} = 1 - \frac{\Gamma(a_r, b_r x^{1/(a_r-b_r)})}{\Gamma(a_r)} = \frac{\gamma(a_r, b_r x^{1/(a_r-b_r)})}{\Gamma(a_r)}, \quad (142)$$

where  $\Gamma(x, y)$  and  $\gamma(x, y)$  are the upper and lower incomplete Gamma functions, respectively.

The corresponding halo density profile  $\rho_h(x)$  is given by

$$\rho_h(x) = \frac{m_h P_r(x)}{4\pi r_s^3 x^2} = \frac{m_h}{4\pi r_s^3} \frac{b_r^{a_r}}{\Gamma(a_r)(a_r - b_r)} \exp\left(-b_r x^{\frac{1}{a_r-b_r}}\right) x^{\frac{3b_r-2a_r}{a_r-b_r}}, \quad (143)$$

or equivalently

$$\rho_h(x) = \rho_s e^{b_r} \exp\left(-b_r x^{\frac{1}{a_r-b_r}}\right) x^{\frac{3b_r-2a_r}{a_r-b_r}} \text{ with } \rho_s = \rho_h(x=1). \quad (144)$$

It can be verified that for inner profile  $\rho_h(r < r_s) \propto r^{(3\gamma_h-2)/(1-\gamma_h)}$ . The halo deformation rate parameter  $\gamma_h$  is related to the new density profile as  $\gamma_h = b_r/a_r$ .

The density profile proposed in Eqs. (143) or (144) is general with four parameters ( $\rho_s$ ,  $r_s$ ,  $a_r$  and  $b_r$ ). For  $\gamma_h = b_r/a_r = 2/3$ , Eq. (144) exactly reduces to Einasto profile (Eq. (S11)) with the Einasto shape parameter  $\alpha = 2/b_r$ . However, the density profile we proposed is a result of the random motion of collisionless particles in a halo with stochastically varying size. The distribution  $P_r(x)$  in Eq. (141) can be interpreted as the probability to find a particle at any position extending to infinity or the distribution of particles in an assembled halo incorporating all possible halos stochastically evolving as Eq. (111). By contrast, the Einasto profile is for individual halos of finite

size. Therefore, parameters of Eq. (144) may have different values from the Einasto profile for individual halos (as shown in Fig. 7).

The number density  $P_r(x)$  in Eq. (141) describes the radial density of collisionless particles from all halos with different sizes evolving according to Eq. (111). The distribution  $P_r(x=r/r_s)$  is defined for all  $x \geq 0$  extending to infinity. Note that this density describes the probability distribution of all particles in all possible halos. It is different from the usual density profiles for individual or stacked halos that have a finite size.

In simulation, instead of working with the spherical averaged halo density profile for each individual halo with a finite size, we compute the density profile for a group of halos of same mass. The function  $F_r(r)$  was computed for a halo group of size  $n_p$  at a given scale factor  $a$ , where  $r$  is the distance of every particle in the halo group to the respective center of mass of the halo that it belongs to. In simulation, the cumulative function  $F_r(r)$  is computed as the fraction of all particles in the same halo group with a distance smaller than  $r$ . The radial density profile  $P_r(x=r/r_s)$  (particle distribution probability) can be obtained by taking the derivative  $\partial F_r(x)/\partial x$  (Eq. (142)). This procedure will significantly reduce the noise as the number of particles in the entire halo group is much greater than the number of particles in individual halos.

Figure 6 plots the log-log variation of the radial cumulative distribution function  $F_r(r=xr_s)$  for all particles in the same halo group of size  $n_p$  at  $z=0$ . Symbols plot the simulation data for five different sizes of halo groups, while the solid lines plot the best fit of the simulation data for each size of halo group using the proposed model Eq. (142) with three free parameters  $r_s$ ,  $a_r$ , and  $b_r$ . The fitted values of three parameters varying with group size  $n_p$  are presented in Figs. 7 and 8.

Clearly, the scaling  $F_r(x=r/r_s) \sim x^3$  for small  $x$  indicates the existence of a central core at halo center (Table 1). The proposed model Eq. (142) provides very good agreement with the simulation data for a wide range of halo group size.

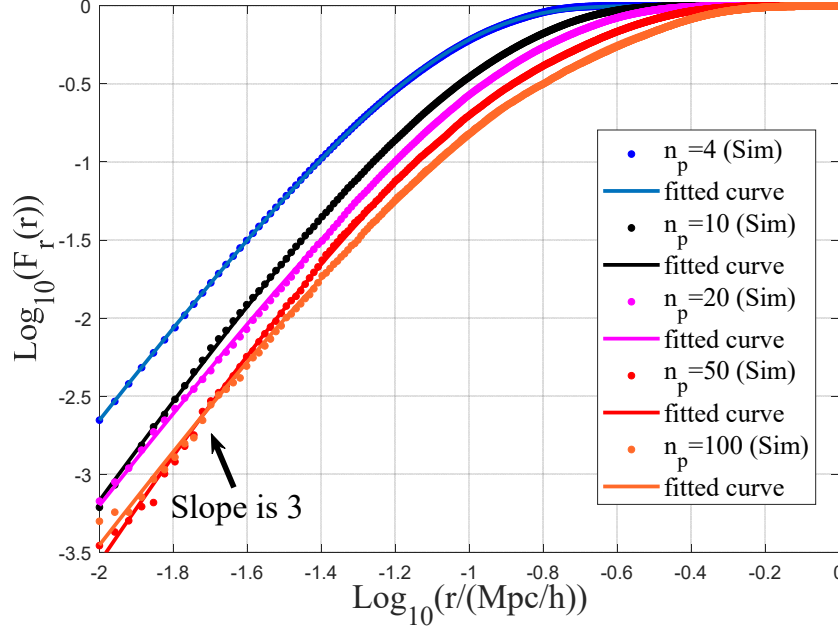


Figure 6. The log-log variation of the cumulative distribution function  $F_r(r = xr_s)$  with the distance  $r$  to the center of mass of the halo that particle belongs to. Function  $F_r(r = xr_s)$  is computed based on all particles in a halo group of the same size  $n_p$  at  $z=0$ . Symbols of dot present the simulation data for five different sizes of halo groups. Solid lines plot the best fit of the simulation data for each size of halo group using the proposed model (Eq. (142)) with three free parameters  $r_s$ ,  $a_r$ , and  $b_r$ . The fitted values of these parameters are presented in next two figures. The scaling  $F_r(x=r/r_s) \sim x^3$  for small  $x$  indicates the existence of a central core at halo center.

Figure 7 presents the variation of fitted values of  $a_r$  and  $b_r$  for  $F_r(r = xr_s)$  with the halo group size  $n_p$ . Both values of  $a_r$  and  $b_r$  slowly increase with the halo size  $n_p$ . However, the ratio of  $a_r/b_r \approx 3/2$  is found for all halo sizes, regardless of the halo size, which is required by a finite density at halo center (Eq. (144)). The exponent parameter  $\alpha_r = 1/(a_r - b_r)$  slowly decreases with

the halo size from 1.2 to 0.7, which is significantly larger than the shape parameter  $\alpha \approx 0.2$  of Einasto profile for individual halos with finite size.

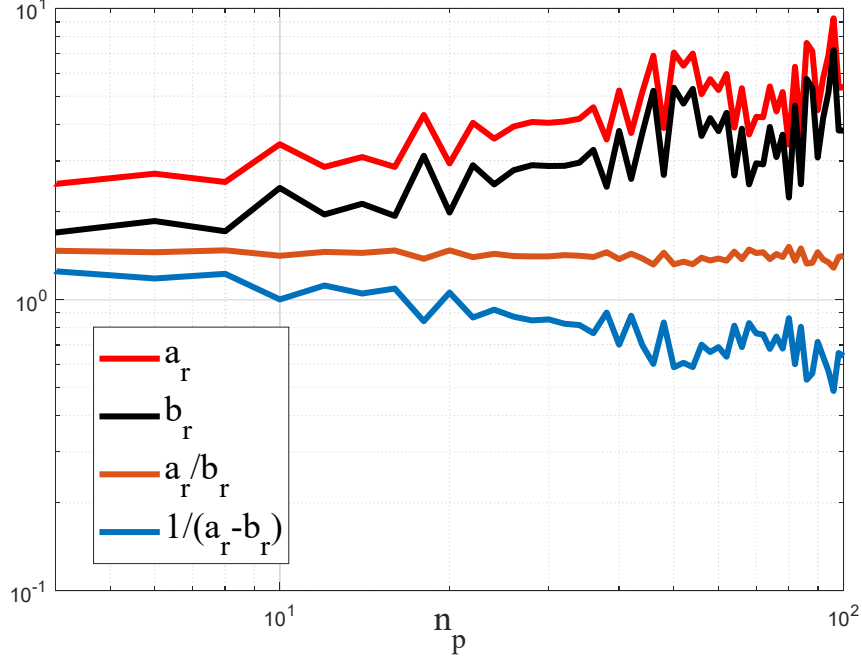


Figure 7. The variation of the fitted values of  $a_r$  and  $b_r$  for cumulative distribution function  $F_r(r = xr_s)$  with halo group size  $n_p$ . Both values of  $a_r$  and  $b_r$  increase with the size  $n_p$ . However, the ratio of  $a_r/b_r \approx 3/2$  is found regardless of the halo size, as required by a finite density at halo center. The exponent parameter  $\alpha_r = 1/(a_r - b_r)$  slowly decreases with the halo size from 1.2 to 0.7. This value is significantly larger than the shape parameter of  $\alpha \approx 0.2$  for an Einasto profile of individual halos with a finite size.

The  $k$ th moment of distribution  $P_r(x)$  can be easily found as

$$M_k = \int_0^\infty P_r(x) x^k dx = \frac{\Gamma(a_r + (a_r - b_r)k)}{b_r^{(a_r - b_r)k} \Gamma(a_r)}. \quad (145)$$

The momentum generating function of the distribution  $P_r(x)$  reads

$$MGF(t) = \int_0^\infty P_r(x) e^{tx} dx = \sum_{k=0}^\infty \frac{t^k \Gamma(a_r + (a_r - b_r)k)}{k! b_r^{(a_r - b_r)k} \Gamma(a_r)}, \quad (146)$$

from which the halo mean square radius  $r_g$  (the root mean square distance) reads

$$r_g = r_s \sqrt{\frac{b_r^{-2(a_r-b_r)} \Gamma(3a_r - 2b_r)}{\Gamma(a_r)}}. \quad (147)$$

Three characteristic length scales can be identified from the simulation data for group of halos of the same mass. The scale radius (halo core size)  $r_s$  can be found by fitting Eq. (142) to the simulation data of  $F_r(r = xr_s)$  in Fig. 6. The mean square radius of halo group can be computed,

$$r_g = \sqrt{\sum_{m=1}^{n_h} \sum_{k=1}^{n_p} (r_{km}^2)} / (n_p n_h), \quad (148)$$

where  $r_{km}$  is the distance of the  $k$ th particle in  $m$ th halo of the halo group to the center of that halo.

Here  $n_h$  is the number of halos in the group. The virial radius  $r_{h\Delta}$  of a halo group can be found

from the simulation data of  $F_r(r = xr_s)$  as

$$\frac{F_r(r_{h\Delta})}{r_{h\Delta}^3} = \frac{4\pi\Delta_c \bar{\rho}(a)}{3m_h}, \quad (149)$$

where  $\bar{\rho}(a)$  is the mean background density at scale factor  $a$ .

Figure 8 plots the variation of three characteristic length scales (in the unit of Mpc/h) with the halo group size  $n_p$ , i.e. the virial radius  $r_{h\Delta}$  with  $\Delta_c = 178$  (Eq. (149)), the mean square radius  $r_g$  (Eq. (148)), and the scale radius  $r_s$  (fitted from the simulation data in Fig. 6). The ratios between three halo sizes are also presented. Note that all three length scales are defined based on the statistics of the entire halos group, instead of individual halos.

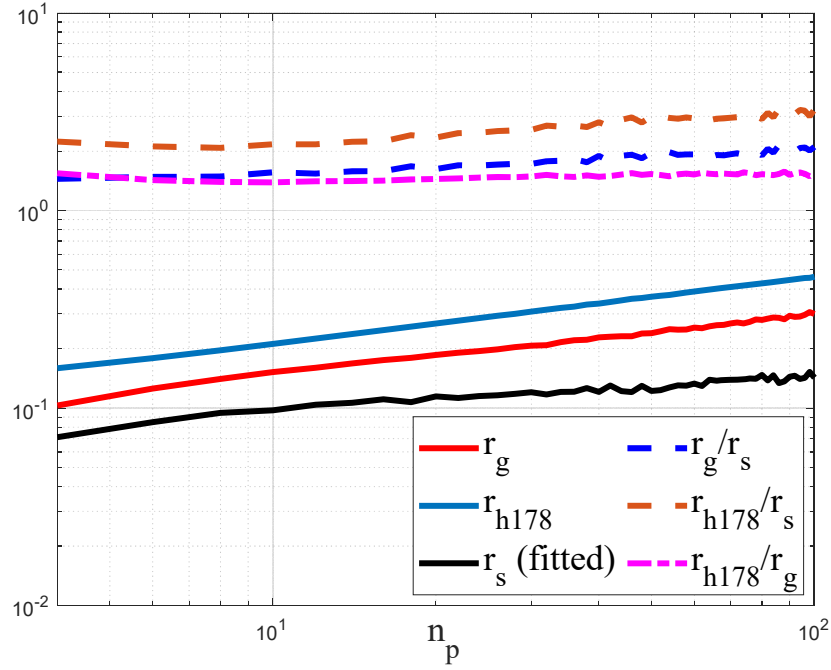


Figure 8. The variation of three length scales (in the unit of Mpc/h) with halo group size  $n_p$ , i.e. the virial radius  $r_{h\Delta}$  with  $\Delta=178$  (Eq. (149)), the mean square radius  $r_g$  (Eq. (148)), and the scale radius  $r_s$  (fitted from the simulation data in Fig. 6).

Finally, all other relevant halo quantities can be obtained with number density  $P_r(x)$  from Eq.

(141). Examples are the mean radial flow  $u_h(x)$  from Eq. (126),

$$u_h(x) = x - (a_r - b_r) b_r^{-a_r} \exp\left(b_r x^{\frac{1}{a_r - b_r}}\right) x^{\frac{-b_r}{a_r - b_r}} \gamma\left(a_r, b_r x^{\frac{1}{a_r - b_r}}\right). \quad (150)$$

The shifted potential  $\phi_h^*(x, a)$  from Eq. (58),

$$\phi_h^*(x, a) = \frac{Gm_h(a)}{\Gamma(a_r) r_s(a)} \left[ b_r^{a_r - b_r} \gamma\left(b_r, b_r x^{\frac{1}{a_r - b_r}}\right) - \frac{1}{x} \gamma\left(a_r, b_r x^{\frac{1}{a_r - b_r}}\right) \right]. \quad (151)$$

The lower incomplete Gamma function has the properties that

$$\gamma(x, y) = \Gamma(x) \text{ for } y \rightarrow \infty \text{ and } \gamma(x, y) = y^x/x \text{ for } y \rightarrow 0, \quad (152)$$

where the shifted potential  $\phi_h^*(x, a)$  simplifies to

$$\phi_h^*(x \rightarrow \infty) = \frac{Gm_h(a)}{r_s(a)} \frac{b_r^{a_r-b_r} \Gamma(b_r)}{\Gamma(a_r)}, \quad (153)$$

$$\phi_h^*(x \rightarrow 0) = \frac{Gm_h(a)}{r_s(a)} \frac{b_r^{a_r} (a_r - b_r)}{a_r b_r \Gamma(a_r)} x^{\frac{b_r}{a_r-b_r}}. \quad (154)$$

#### 4.3. Equation of state for relative pressure and density

The velocity dispersion  $\sigma_{nr}^2$  can be obtained with Eqs. (68) and  $F_r(x)$  from (142). It should be interesting to examine the equation of state (EOS) in the core region, where halo density is approximately

$$\rho_h(x) = \rho_h(0) \left( 1 - b_r x^{\frac{2}{b_r}} \right) \quad \text{and} \quad \rho_h(0) = \frac{m_h}{4\pi r_s^3} \frac{b_r^{a_r}}{\Gamma(a_r)(a_r - b_r)} \quad (155)$$

from Eq. (144) with  $a_r = 3b_r/2$  for small  $x$ . From Eqs. (64) and (65), pressure in core region is,

$$p_h(x) = \rho_h(x) \sigma_r^2(x) = p_h(x=0) - \frac{1}{2} \frac{\rho_h^2(0) v_{cir}^2}{\bar{\rho}_h c^2} x^2. \quad (156)$$

The Equation of state in the core region can be finally written as (with Eq. (155)),

$$[p_h(0) - p_h(x)] = \frac{[\rho_h(0)]^{2-b_r} v_{cir}^2}{2(b_r)^{b_r} \bar{\rho}_h c^2} [\rho_h(0) - \rho_h(x)]^{b_r} \quad (157)$$

such that  $\Delta p_h = K_s (\Delta \rho_h)^{b_r}$ . Unlike the ideal gas with reference pressure and density being zero, here each halo has its center pressure and density as a reference where both gravitational and pressure forces vanish. The relative pressure and density  $\Delta p_h$  and  $\Delta \rho_h$  to the center of halo satisfy the equation of state (157). The parameter  $b_r$  has the physical meaning as the exponent of equation



of state. Note that for regular polytropic model  $p_h \propto \rho_h^{1+1/n}$  with an index  $n$ , from Lane-Emden equation, the relative pressure and density in the core region always satisfy  $\Delta p_h \propto \Delta \rho_h$  (or  $b_r = 1$ ) regardless the value of  $n$ . This indicates that the regular polytropic equation of state for absolute pressure and density may not applicable to dark matter halos. Figure 7 shows that the value of  $b_r$  slightly increases from 1.5 to 3 with increasing halo group size. The NFW profile will not lead to such equation of state because of divergent pressure/density fields (Eqs. (69) and (70)).

Let's assume the equilibrium center pressure and density are  $p_h(0)$  and  $\rho_h(0)$ , where both gravitational and pressure forces are not present. At any location in halo, the relative pressure  $\Delta p_{hn}$  and  $\Delta \rho_{hn}$  (normalized and using Eqs. (67), (33), and (16)) can be written in terms of  $F_r(x)$ ,

$$\Delta p_{hn} = \frac{p_h(0) - p_h(x)}{(r_s^2/t^2)(m_h/4\pi r_s^3)} = \frac{4\pi^2}{F_r(1)} \int_0^x \frac{F_r(x) F_r'(x)}{x^4} dx - \int_0^x \frac{F_r^2(x) F_r''(x)}{x^2 [F_r'(x)]^2} dx \quad (158)$$

and

$$\Delta \rho_{hn} = \frac{\rho_h(0) - \rho_h(x)}{(m_h/4\pi r_s^3)} = \left[ \frac{F_r'(x)}{x^2} \right]_{x=0} - \frac{F_r'(x)}{x^2}. \quad (159)$$

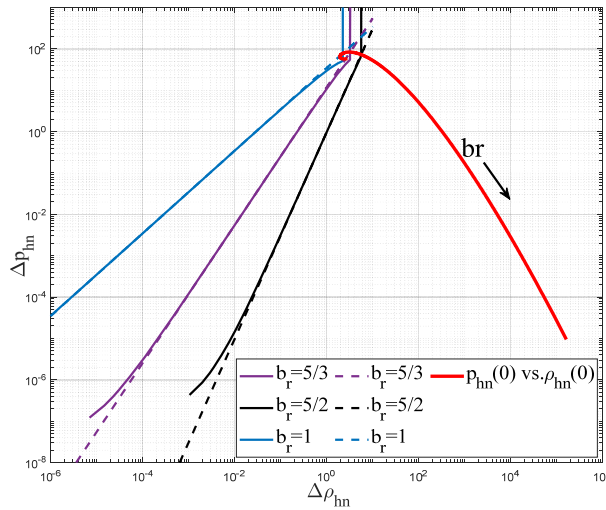


Figure 9. The variation of relative pressure  $\Delta p_{hn}$  with relative density  $\Delta \rho_{hn}$  for different exponents  $b_r$ . The proposed model yields an equation of state  $\Delta p_{hn} \propto (\Delta \rho_{hn})^{b_r}$  that can be clearly identified (solid lines). The analytical equation of state (160) is plotted as dash lines for comparison. The relation (Eq. (161)) between center pressure  $p_{hn}(0)$  and center density  $\rho_{hn}(0)$  is presented as the red solid line for different  $b_r$  (i.e. the maximum  $\Delta p_{hn}$  vs. maximum  $\Delta \rho_{hn}$ ). The center velocity dispersion  $\sigma_{r0}^2$  can be identified accordingly.

More specifically with  $F_r(x)$  from Eq. (142) and  $a_r = 3b_r/2$ , equation of state (157) reduces to

$$\Delta p_{hn} = \frac{2^{3-b_r} \pi^2 (b_r)^{3b_r-2-3b_r^2/2}}{3\gamma(3b_r/2, b_r) \Gamma(3b_r/2)^{1-b_r}} (\Delta \rho_{hn})^{b_r}, \quad (160)$$

where  $\gamma(x, y)$  is the lower incomplete Gamma functions. Let's assume the equation of state (157) is valid for the entire range of  $x$  extending to infinity. By setting  $p_h(\infty) = 0$  and  $\rho_h(\infty) = 0$ , a simple relation (regardless of the value of  $b_r$ ) between center pressure and density is obtained,

$$p_h(0) = \frac{v_{cir}^2}{2(b_r)^{b_r} \bar{\rho}_h c^2} \rho_h^2(0) = \frac{2\pi G r_s^2}{3(b_r)^{b_r}} \rho_h^2(0) = K_r(a) \rho_h^2(0), \quad (161)$$

where the pre-factor  $K_r(a) \approx 0.01aG(1Mpc/h)^2$  should be independent of halo mass  $m_h$ . At the same redshift  $z$  (or  $a$ ) and with  $r_s \propto m_h^{1/3}$  increasing with halo mass  $m_h$ ,  $b_r$  is also expected to be slightly increasing with halo mass  $m_h$ . On the other hand,

$$p_h(0) = \frac{v_{cir}^2}{2(b_r)^{b_r} \bar{\rho}_h c^2} \rho_h^2(0) = \frac{Gm_h}{3r_s} \frac{(b_r)^{b_r/2-1}}{\Gamma(3b_r/2)} \rho_h(0) = \sigma_{r0}^2(m_h, a) \rho_h(0), \quad (162)$$

where  $\sigma_{r0}^2 = \sigma_r^2(x=0)$  is the center velocity dispersion and  $\sigma_{r0}^2 \propto m_h^{2/3} a^{-1}$ . For  $b_r = 5/3$  (exponent for adiabatic process),  $\sigma_{r0}^2 \approx 26 r_s^2 / t^2$  compared to  $\sigma_{r0}^2 = 2\pi^2 c^2 r_s^2 / t^2$  for isothermal profile. With  $p_h(0)$  from Eq. (161), the core size (where Hubble flow is dominant)  $x_c = (b_r)^{-b_r/2}$

(in Eq. (66)) can be easily obtained by forcing  $p_h(x) = 0$  in Eq. (156). The core size  $x_c = 1$  for  $b_r = 0$  (core size exactly equals scale radius) and decreases for with  $b_r$ . For  $b_r = 5/3$ ,  $x_c \approx 0.65$ .

Figure 9 summarizes the equation of state for relative pressure and density. With cumulative function  $F_r(x)$  from Eq. (142), the variation of relative pressure  $\Delta p_{hn}$  with relative density  $\Delta \rho_{hn}$  is plotted for different  $b_r$  using Eqs. (158) and (159). Clearly, equation of state follows a scaling law  $\Delta p_{hn} \propto (\Delta \rho_{hn})^{b_r}$  for most range of density, while deviation is only observed in the outer halo region with low density. Analytical approximation (dash lines from Eq. (160)) is presented for comparison. The relation between center pressure and density is also plotted as red thick line. Figure 10 plots the variation of center density  $\rho_h(0)$ , center pressure  $p_h(0)$ , and center dispersion  $\sigma_{r0}^2$  with exponent  $b_r$ . For  $b_r \rightarrow 0$ , the velocity dispersion  $\sigma_{r0}^2 \approx 20 r_s^2 / t^2$ . There exist a minimum  $\rho_h(0)$ , a maximum  $p_h(0)$  and maximum  $\sigma_{r0}^2$  at certain values of  $b_r$ .

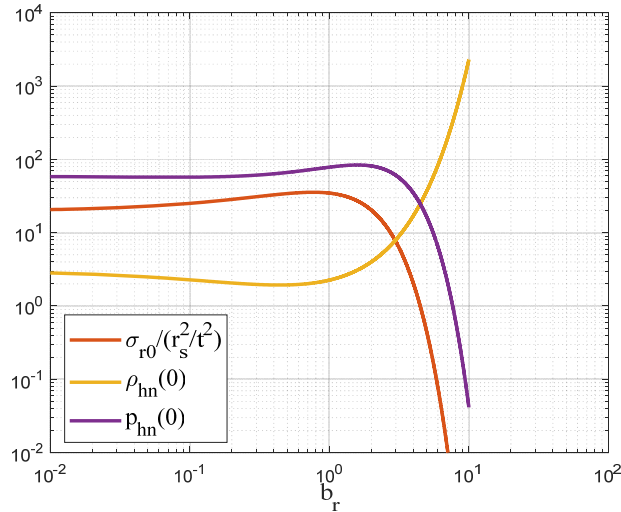


Figure 10. The variation of normalized relative pressure  $\Delta p_{hn}$  (Eq. (162)), relative density  $\Delta \rho_{hn}$  (Eq. (155)), and center dispersion  $\sigma_{r0}^2 / (r_s^2 / t^2)$  for different parameter  $b_r = 2/\alpha$ , where  $\alpha$  is the shape parameter. There exist a maximum  $\Delta p_{hn}$ , minimum  $\Delta \rho_{hn}$  and maximum center dispersion at certain values of  $b_r$ .

#### 4.4. Simple closures for self-consistent particle distribution

The relation between radial  $u_h(x)$  and osmotic velocity  $u_h^*(x)$  is presented in Eq. (129). The particle distribution function  $P_r(x)$  can be fully determined if an additional closure can be introduced to relate  $u_h(x)$  and  $u_h^*(x)$ , which is the focus of this section. The other option is to use equation of state as an additional closure. See supplementary information.

### 5. Conclusion

The gravitational collapse of collisionless particles is essentially a nonlinear self-gravitating collisionless fluid flow problem (SG-CFD). The inverse mass cascade is a unique feature of SG-CFD that shares many similarities with the inverse energy cascade of two-dimensional turbulence. This paper focus on the inverse mass cascade and its direct effects on relevant halo properties and internal structures, as halos are intrinsically dynamical objects that mediate the mass cascade.

The halo internal structure is highly dependent on mass cascade. The continuous mass accretion creates a new layer of mass that deforms the original halo and creates a non-zero mean radial flow (Figs. 1 and 2, and Eq. (24), outflow for core region and inflow for outer region). Isothermal density is a natural result of a vanishing mean radial flow (Eq. (25)). The combined in- and out-flow leads to an extra length scale (the scale radius  $r_s$ ) for density profile where mass flow is at its maximum. A double-power-law density (Eqs. (39) and (42)) is proposed with inner density dominated by the halo deformation rate  $\gamma_h$  and outer density controlled by a halo deformation parameter  $\alpha_h$  that is dependent on halo concentration, and mass cascade parameters  $\lambda$  and  $\tau_0$  (Eq. (14)). The cusp-core controversy will depend on the deformation rate (the gradient of mean

radial flow)  $\gamma_h$  at halo center. Slower deformation leads to a steeper core density profile (Eq. (39)). For large halos with extremely fast mass accretion and an expanding core, Hubble flow is expected at halo center that hints the existence of a central halo core with  $\gamma_h = 2/3$  (Eq. (40)).

The momentum and energy exchange between the mean flow and velocity dispersion (random motion) is studied via the Jeans' equation (Eq. (59)) for spherical non-rotating isotropic halos. The radial flow is shown to enhance the radial random motion in outer region (Fig. 4). The closure problem of halo density profile can be reduced to the correct modeling of radial flow  $u_h(x)$ . The halo density profile is derived for a given Taylor expansion of  $u_h(x)$  around  $x = 0$ . The critical halo concentration  $c = 3.48$  is obtained as a result of vanishing linear radial momentum for large halos (Fig. 3 and Eq. (53)). A complete analysis of the effects of radial flow on various halo energies is also presented (Eqs. (79)-(90)). Halo surface energy and surface tension are introduced for halos with finite size as extra energy is required to create the expanding surface (Eqs. (94) and (95)). An effective exponent  $n_e$  of gravitational interaction is discovered with an estimate value of  $n_e = -1.3$  (deviate from the usual exponent -1.0 for gravity) to reflect the effects of mass cascade and surface energy of halos (Eq. (101)).

Halos are dynamically evolving due to inverse mass cascade. New stochastic models are formulated for the random evolution of halo size that follows a geometric Brownian motion (Eqs. (111)). As a result, halo size follows a lognormal distribution (Eq. (115)). Stochastic models are also developed for the random motion of collisionless particles in stochastically evolving halos (Eqs. (122) and (123)). This model involves drift terms including both mean radial and osmotic flow ( $u_h$  and  $u_h^*$ ) and a multiplicative noise term due to the random halo size. The solution of that model leads to the relation between particle density distribution  $P_r$  (the probability to find a

particle at a given position) and the mean radial and osmotic flow (Eqs. (126) and (127)). It is demonstrated that the closure problem of halo density profile can be equivalently reduced to a correct modeling of either the mean flow  $u_h$ , or the osmotic flow  $u_h^*$ , or identifying an additional closure between  $u_h$  and  $u_h^*$  besides Eq. (129).

In this work, a simple model of osmotic flow  $u_h^*$  (Eq. (136)) is proposed such that the radial particle distribution function  $P_r$  can be fully derived (Eq. (141)), as well as other relevant halo properties (Eq. (143) for particle density distribution, Eq. (150) for radial flow, and Eq.(151) for shifted potential). The proposed model provides an excellent fit to the cumulative function of particle density  $F_r$  that is computed for halo groups of different sizes from a N-body simulation. The model agrees with a very wide range of halo group sizes, where a central halo core exists with  $F_r(x) \sim x^3$  due to the Hubble radial flow at halo center (Fig. 6). With reference pressure and density defined at halo center where both gravitational and pressure forces are absent, equation of state for relative pressure and density is established based on this model (Fig. 9 and Eqs. (157) and (160)). The pressure, density, and velocity dispersion at halo center are also presented (Fig. 10 and Eqs. (161) and (162)). A simple closure between  $u_h$  and  $u_h^*$  is proposed for a self-consistent particle distribution function in supplemental information (Eq. (S20)).

In short, inverse mass cascade is a fundamental feature of SG-CFD. Its effects on the structure formation and evolution remain an important topic. Some examples of future work are briefly discussed here. The concentration-mass relation (the mass dependence of  $c$ ) might be related to the mass dependence of  $\alpha_h$  and/or  $\lambda$ , with Eq. (14) providing a relation between concentration  $c$ , deformation parameter  $\alpha_h$  and mass cascade parameter  $\lambda$  and  $\tau_0$ . Further study is also desired for identifying a better closure to better understand the origin of universal halo structures.

## References

1. Lukic, Z., et al., *The halo mass function: High-redshift evolution and universality*. Astrophysical Journal, 2007. **671**(2): p. 1160-1181.
2. Neyman, J. and E.L. Scott, *A Theory of the Spatial Distribution of Galaxies*. Astrophysical Journal, 1952. **116**(1): p. 144-163.
3. Cooray, A. and R. Sheth, *Halo models of large scale structure*. Physics Reports-Review Section of Physics Letters, 2002. **372**(1): p. 1-129.
4. Richardson, L.F., *Weather Prediction by Numerical Process*. 1922, Cambridge, UK: Cambridge University Press.
5. Kraichnan, R.H., *Inertial Ranges in 2-Dimensional Turbulence*. Physics of Fluids, 1967. **10**(7): p. 1417-+.
6. Press, W.H. and P. Schechter, *Formation of Galaxies and Clusters of Galaxies by Self-Similar Gravitational Condensation*. Astrophysical Journal, 1974. **187**(3): p. 425-438.
7. Bond, J.R., et al., *Excursion Set Mass Functions for Hierarchical Gaussian Fluctuations*. Astrophysical Journal, 1991. **379**(2): p. 440-460.
8. Tomita, K., *Formation of Gravitationally Bound Primordial Gas Clouds*. Progress of Theoretical Physics, 1969. **42**(1): p. 9-&.
9. Gunn, J.E. and J.R. Gott, *Infall of Matter into Clusters of Galaxies and Some Effects on Their Evolution*. Astrophysical Journal, 1972. **176**(1): p. 1-&.
10. Sheth, R.K., H.J. Mo, and G. Tormen, *Ellipsoidal collapse and an improved model for the number and spatial distribution of dark matter haloes*. Monthly Notices of the Royal Astronomical Society, 2001. **323**(1): p. 1-12.
11. Sheth, R.K. and G. Tormen, *Large-scale bias and the peak background split*. Monthly Notices of the Royal Astronomical Society, 1999. **308**(1): p. 119-126.
12. Del Popolo, A. and P. Kroupa, *Density profiles of dark matter haloes on galactic and cluster scales*. Astronomy & Astrophysics, 2009. **502**(3): p. 733-747.
13. Moore, B., et al., *Resolving the structure of cold dark matter halos*. Astrophysical Journal, 1998. **499**(1): p. L5-+.
14. Klypin, A., et al., *Resolving the structure of cold dark matter halos*. Astrophysical Journal, 2001. **554**(2): p. 903-915.
15. Navarro, J.F., C.S. Frenk, and S.D.M. White, *A universal density profile from hierarchical clustering*. Astrophysical Journal, 1997. **490**(2): p. 493-508.
16. Navarro, J.F., et al., *The inner structure of  $\Lambda$ CDM haloes - III. Universality and asymptotic slopes*. Monthly Notices of the Royal Astronomical Society, 2004. **349**(3): p. 1039-1051.
17. Xu, Z., *Inverse mass cascade of self-gravitating collisionless flow and effects on halo mass functions*. arXiv:2109.09985 [astro-ph.CO], 2021.
18. C. S. Frenk, et al., *Public Release of N-body simulation and related data by the Virgo consortium*. arXiv:astro-ph/0007362v1 2000.
19. Jenkins, A., et al., *Evolution of structure in cold dark matter universes*. Astrophysical Journal, 1998. **499**(1): p. 20.
20. Colberg, J.M., et al., *Linking cluster formation to large-scale structure*. Monthly Notices of the Royal Astronomical Society, 1999. **308**(3): p. 593-598.
21. Einasto, J., et al., *Structure of Superclusters and Supercluster Formation .3. Quantitative Study of the Local Supercluster*. Monthly Notices of the Royal Astronomical Society, 1984. **206**(3): p. 529-558.
22. Zhao, D.H., et al., *Accurate Universal Models for the Mass Accretion Histories and Concentrations of Dark Matter Halos*. Astrophysical Journal, 2009. **707**(1): p. 354-369.

23. Correa, C.A., et al., *The accretion history of dark matter haloes - III. A physical model for the concentration-mass relation*. Monthly Notices of the Royal Astronomical Society, 2015. **452**(2): p. 1217-1232.
24. Gao, L., et al., *The redshift dependence of the structure of massive Lambda cold dark matter haloes*. Monthly Notices of the Royal Astronomical Society, 2008. **387**(2): p. 536-544.
25. Binney, J. and G.A. Mamon, *M/L and Velocity Anisotropy from Observations of Spherical Galaxies, or Must M87 Have a Massive Black-Hole*. Monthly Notices of the Royal Astronomical Society, 1982. **200**(1): p. 361-375.



Supplementary information for  
Inverse mass cascade of self-gravitating collisionless flow and effects on  
halo deformation, energy, size, and density profiles

Zhijie (Jay) Xu<sup>1,a</sup>

1. Computational Mathematics Group, Physical and Computational Sciences Directorate, Pacific  
Northwest National Laboratory, Richland, WA 99352, USA

---

<sup>a)</sup> Electronic mail: [zhijie.xu@pnnl.gov](mailto:zhijie.xu@pnnl.gov); [zhijiexu@hotmail.com](mailto:zhijiexu@hotmail.com)

Contents	
Nomenclature .....	3
The simulation data .....	8
Halo density profiles .....	9
The NFW density profile .....	9
The power-law density profile .....	10
The Einasto density profile .....	11
Simple closures for self-consistent particle distribution .....	12
Supplementary figures.....	18

## Nomenclature

Symbol	S.I. Unit	Physical Meaning
$\Omega_0$	Dimensionless	Matter content
$\Lambda$	$1/m^2$	Universe constant
$h$	Dimensionless	Dimensionless Hubble constant
$\Gamma$	Dimensionless	$\Gamma = \Omega_0 h$ Shape parameter for the density power spectrum
$\sigma_8$	Dimensionless	Density fluctuation at $r = 8Mpc/h$
$L$	$m$	Size of the simulation box
$N$	Dimensionless	Total number of particles in the simulation
$m_p$	$kg$	Mass of a collisionless particle in simulation (mass resolution)
$l_{soft}$	$m$	Gravitational softening length
$V$	$m^3$	Volume of the simulation box
$n$	Dimensionless	Exponent of the interaction potential. Specifically, $n=-1$ represents the usual gravitational interaction.
$n_{ps}$	Dimensionless	Effective index of power spectrums of density fluctuations
$G$	$m^3/(kg \cdot s^2)$	Gravitational constant
$a, z$	Dimensionless	Scale factor and redshift $a = 1/(1+z)$
$H_0, H$	$1/s$	Hubble constants ('0' stands for the present epoch)
$t_0, t$	$s$	Physical time (0' stands for the present epoch)
$N_h$	Dimensionless	Total number of halos in the system
$M_o(a)$	$kg$	Total mass of out-of-halo subsystem
$M_h(a)$	$kg$	Total mass of halo subsystem
$m_g(m_h, a)$	$kg$	Total mass of a halo group of halos with the same mass $m_h$
$m_h$	$kg$	Mass of a given halo
$n_h$	Dimensionless	Number of halos in a halo group
$n_p$	Dimensionless	Number of particles in a halo
$m_h^*$	$kg$	Characteristic mass scale
$m_h^L$	$kg$	Mass of a typical large halo
$r_h$	$m$	The virial radius (size) of spherical halos
$D_{FM}$	Dimensionless	Forward mass redistribution function
$D_{BM}$	Dimensionless	Backward mass redistribution function
$D_{NM}$	Dimensionless	Net mass redistribution function

$\Pi_m(m_h, a)$	$kg/s$	Mass flux function
$\varepsilon_m(a)$	$kg/s$	Mass flux function for mass propagation range
$f_M(m_h, m_h^*)$	$1/kg$	Halo mass function
$T_m(m_h, a)$	$1/s$	Real-space mass transfer function
$\tau_h(m_h, a)$	$s$	Time interval of a single merging for a halo group of size $m_h$
$f_h(m_h, a)$	$1/s$	Frequency of halo merging for a halo group of size $m_h$
$f_0(a)$	$1/s$	Fundamental frequency of halo merging
$\tau_M(a)$	$s$	Time to cascade the entire mass in halo sub-system
$\tau_f(m_h, a)$	$s$	Average time to form a halo of mass $m_h$
$\tau_g(m_h, a)$	$s$	Mean time to cascade mass of a halo group of size $m_h$
$\tau_{gr}$	$s$	Random waiting time for a halo of mass $m_h$
$\tau_h^*(a)$	$s$	Characteristic time scale for a halo of mass $m_h^*$
$n_p^*, n_p^L$	Dimensionless	Number particles in a halo of mass $m_h^*$ and $m_h^L$
$n_h^*, n_h^L$	Dimensionless	Number of halos in a halo group of size $m_h^*$ and $m_h^L$
$m_g^*$	$kg$	Total mass of a halo group of size $m_h^*$
$m_g^c(m_h)$	$kg$	Critical group mass required to sustain mass propagation
$\alpha_0$	Dimensionless	Numerical constant for the mass flux function (order of unity)
$\beta_0$	Dimensionless	Numerical constant for the halo mass function
$\lambda_0$	Dimensionless	Numerical constant for the total mass of halo sub-system
$\tau_0$	Dimensionless	Scaling exponent for the fundamental frequency $f_0(a)$
$b_0$	Dimensionless	Mass resolution parameter for the fundamental frequency $f_0(a)$
$c_0$	Dimensionless	Constant $c_0 = b_0 \lambda_0$ for the mass fraction of a halo sub-system
$\gamma_0$	Dimensionless	Numerical constant for the mean square mass
$\eta_0$	Dimensionless	Numerical constant for the mass deposition range
$\lambda$	Dimensionless	Halo geometry parameter
$D_h$	Dimensionless	Halo fractal dimension
$P_h(m_h, t)$	$1/kg$	Distribution function of a random walk in halo mass space
$D_p(m_h)$	$kg^2/s$	Position-dependent diffusivity for a random walk in halo mass space $D_p(m_h) = D_{p0} m_h^{2\lambda}$
$D_{p0}$	$kg^{2(1-\lambda)}/s$	Proportional constant for $D_p(m_h)$
$\alpha_p$	Dimensionless	Dimensionless constant for position-dependent diffusivity

$\xi(t)$	Dimensionless	Jumping length in halo mass space
$D_{dp}(a)$	$kg^2$	Mass space diffusivity in mass propagation range
$D_{md}(a)$	$kg^2$	Mass space diffusivity in mass deposition range
$D_{m0}$	$kg^{2(1-\lambda)}$	Proportional constant for $D_{md}(a)$
$v$	Dimensionless	Normalized variable for halo mass function
$\bar{\rho}_0$	$kg/m^3$	The physical background density at the current epoch
$n_e$	Dimensionless	The effective exponent of gravitational potential $V_p(r) \sim r^{n_e}$
$\delta_c(a)$	Dimensionless	The critical density from a spherical collapse model
$\sigma_v^2(m_h)$	$m^2/s^2$	The halo virial velocity dispersion for halos of mass $m_h$
$r_s$	$m$	Scale radius where the logarithmic slope of halo density is -2
$c$	Dimensionless	Halo concentration parameter $c = r_h/r_s$
$\rho_h(r)$	$kg/m^3$	Halo density profile as a function of distance $r$ from the center
$\bar{\rho}_h$	$kg/m^3$	Mean halo density
$\bar{\rho}_r(r)$	$kg/m^3$	Mean density within a sphere of radius $r$
$\rho_s$	$kg/m^3$	Mass density at the scale radius $\rho_s = \rho_h(r=r_s)$
$\alpha$	Dimensionless	Shape parameter for an Einasto density profile
$v_{cir}$	$m/s$	Circular velocity at the virial radius $r_h$ of halo
$v_c(r, a)$	$m/s$	Circular velocity at radius $r$ , $v_c(r=r_h, a) = v_{cir}$
$N_s$	Dimensionless	Number of particles of mass $m_p$ on the surface of a halo
$\alpha_h$	Dimensionless	Halo deformation parameter
$u_r(r, a)$	$m/s$	Mean halo radial flow velocity
$u_h(x)$	Dimensionless	Normalized halo radial flow velocity
$u_p(x)$	Dimensionless	Normalized halo peculiar radial flow
$x_0$	Dimensionless	The location with $u_h(x) = 0$ and maximum circular velocity $v_c$
$\theta_{vr}$	Dimensionless	Angle between particle peculiar velocity and position vector
$L_{hr}(a)$	$kg \cdot m/s$	Halo radial linear momentum
$K_{hr}(a)$	$kg \cdot m^2/s^2$	Halo radial kinetic energy
$\lambda_{hr}(c)$	Dimensionless	Concentration-dependent coefficient for linear momentum
$\lambda_{Kr}(c)$	Dimensionless	Concentration-dependent coefficient for kinetic energy
$\phi_h(r, a)$	$m^2/s^2$	Halo gravitational potential

$\phi_h^*(r, a)$	$m^2/s^2$	Shifted halo gravitational potential $\phi_h^*(r=0, a)=0$
$\beta_h$	Dimensionless	Anisotropy parameter for halo velocity dispersion
$\sigma_{nr}^2$	Dimensionless	Radial dispersion normalized by the circular velocity $v_{cir}$
$\sigma_{nr1}^2$	Dimensionless	Radial dispersion due to halo mean radial flow
$\sigma_{nr2}^2$	Dimensionless	Radial dispersion due to gravitational interaction
$p_{nr}(x)$	Dimensionless	Normalized halo pressure
$\phi_{nh}(x)$	Dimensionless	Normalized halo gravitational potential
$\rho_{nh}(x)$	Dimensionless	Normalized halo density
$\gamma_h$	Dimensionless	Halo deformation rate parameter
$J_c$	$kg/(ms^2)$	Pressure constant at halo core region
$I_h$	Dimensionless	Normalized first order moment of linear momentum
$S_u$	Dimensionless	Halo surface pressure from mean radial flow
$S_\sigma S_{\sigma1} S_{\sigma2}$	Dimensionless	Halo surface pressure from velocity dispersion
$K_u$	Dimensionless	Halo kinetic energy from mean radial flow
$K_\sigma K_{\sigma1} K_{\sigma2}$	Dimensionless	Halo kinetic energy from velocity dispersion
$\Phi_h$	Dimensionless	Halo gravitational potential
$A_h$	$m^2$	Halo surface area
$S_{eh}$	$kg \cdot m^2/s^2$	Halo surface energy
$S_{th}$	$kg \cdot 1/s^2$	Halo surface tension
$S_{nth}$	Dimensionless	Dimensionless halo surface tension
$\rho_{sur}$	$kg/m^2$	Surface density at the surface of a halo
$\alpha_{st}$	Dimensionless	Numerical constant for halo surface tension
$n_e$	Dimensionless	Effective exponent of gravitational interaction for halos
$b_{rh}$	Dimensionless	Drift constant for stochastic model of halo size evolution
$\alpha_{rh}, \beta_{rh}$	Dimensionless	Constants for multiplicative noise during halo size evolution
$\xi_{rh}, \xi_{rh}^*$	Dimensionless	Noise in the model for particle outward and inward motion
$t_i$	$s$	Initial time $r_h(t_i) = r_{h0}$ for halo size evolution
$r_{h0}$	$m$	Initial halo size for the stochastic equation of halo size
$P_{rh}(r_h, t)$	$1/m$	Probability distribution of halo size $r_h$
$D_{rh}, d_r$	Dimensionless	Diffusivity for the stochastic model of particle motion
$u_h^*(x)$	Dimensionless	The halo osmotic flow
$P_r(x)$	Dimensionless	The radial particle density of a halo group

$\sigma(x)$	Dimensionless	Function for multiplicative noise
$\alpha_r, \beta_r, \gamma_r$	Dimensionless	Parameters for a simple model of the osmotic flow $u_h^*(x)$
$a_r, b_r$	Dimensionless	Parameters for radial particle number density in a halo group
$r_g$	$m$	The mean square radius of a halo group
$r_{h\Delta}$	$m$	The virial radius of a halo group
$\lambda_h$	Dimensionless	Proportional constant between radial and osmotic flow
$d_h$	Dimensionless	Parameter for self-consistent density profile $d_h = d_r / \lambda_h$
$\Delta p_h, \Delta p_{hn}$	$kg / (m \cdot s^2)$	Pressure (and normalized) relative to the center of halo
$\Delta \rho_h, \Delta \rho_{hn}$	$kg / m^3$	Density (and normalized) relative to the center of halo

## The simulation data

The numerical data for this work is publicly available and generated from  $N$ -body simulations carried out by the Virgo consortium, an international collaboration that aims to perform large  $N$ -body simulations for the formation of large-scale structures. A comprehensive description of the simulation data can be found in [1, 2]. As a first step, the current work focus on the matter-dominant gravitational collapse of collisionless particles using simulations where  $\Omega_0 = 1$  and a standard CDM power spectrum (SCDM). A similar analysis can be extended to other simulations with different model assumptions and parameters in the future.

The same set of simulation data has been widely used in a number of different studies from clustering statistics [2] to the formation of halo clusters in large scale environments [3], and testing models for halo abundance and mass functions [4]. The simulation includes over  $N = 256^3$  particles with mass  $m_p = 2.27 \times 10^{11} M_\odot / h$ . The simulation box size is around 240 Mpc/h, where  $h$  is the dimensionless Hubble constant in the unit of  $100 \text{ km/Mpc} \cdot \text{s}$ .

Some key parameters of  $N$ -body simulations are listed in Table S1. The friends-of-friends algorithm (FOF) was used to identify all halos from the simulation data that depends only on a dimensionless parameter  $b$ , which defines the linking length  $b(N/V)^{-1/3}$ , where  $V$  is the volume of the simulation box. Halos were identified with a linking length parameter of  $b = 0.2$  in this work. All halos identified from the simulation data were first grouped into halo groups of different sizes according to halo mass  $m_h$  (or in terms of  $n_p$ , the number of particles in the halos), where  $m_h = n_p m_p$ . The total mass for a halo group of mass  $m_h$  is  $m_g = m_h n_h$ , where  $n_h$  is the number of halos in a given group. Simulation results will be presented to describe the inverse mass cascade across halo groups of different sizes and compared with theory.



Table S1. Numerical parameters of  $N$ -body simulation for SCDM

Run	$\Omega_0$	$\Lambda$	$h$	$\Gamma$	$\sigma_8$	$L(Mpc/h)$	$N$	$m_p(M_\odot/h)$	$l_{soft}(Kpc/h)$
SCDM1	1.0	0.0	0.5	0.5	0.51	239.5	$256^3$	$2.27 \times 10^{11}$	36

## Halo density profiles

### The NFW density profile

Although halos growing via mass accretion is a complex, hierarchical, and nonlinear process, the radial density profile  $\rho_h(r)$  of halos can be robustly fitted by a simple double logarithmic function from cosmological  $N$ -body simulations (NFW profile [5]),

$$\rho_h(r) = \frac{m_h}{4\pi r^3} \frac{1}{F(c)(1+r_s/r)^2} = \frac{\bar{\rho}_r(r)}{3F(r_s/r)(1+r_s/r)^2}. \quad (S1)$$

The logarithm slope of NFW density profile is

$$\frac{d \ln \rho_h}{d \ln r} = -\frac{1+3r/r_s}{1+r/r_s}, \quad (S2)$$

where  $r$  is the distance to the center of halo,  $m_h = m_r(r=r_h)$  is the total mass of a given halo.

Here  $m_r(r)$  is the total mass enclosed within radius  $r$ ,  $\bar{\rho}_r(r) = m_r(r)/(4\pi r^3/3)$  is the mean density within radius  $r$ , and  $r_h$  is the virial radius of the halo in physical coordinates. The scale radius  $r_s$  is defined as the radius where the density profile  $\rho_h(r)$  changes its logarithmic slope from -1 for  $r/r_s \ll 1$  to -3 for  $r/r_s \gg 1$ . The logarithmic slope is exactly -2 at the scale radius  $r_s$ .

The halo concentration parameter  $c = r_h/r_s$  is a key ratio between the halo size and the scale radius that reflects the halo structure. The function  $F(x)$  is defined for NFW profile,

$$F(x) = \ln(1+x) - \frac{x}{1+x}. \quad (\text{S3})$$

The halo mass  $m_r(r)$  within radius  $r$  can be obtained by the integration of density,

$$m_r(r) = \int_0^r \rho_h(y) 4\pi y^2 dy = m_h \frac{F(r/r_s)}{F(r_h/r_s)}. \quad (\text{S4})$$

The density at the surface of halo  $r = r_h$  can be obtained from Eq. (S1),

$$\rho_h(r = r_h) = \frac{m_h}{4\pi r_h^3} \frac{1}{F(c)(1+1/c)^2} = \frac{\bar{\rho}_h}{3F(c)(1+1/c)^2}, \quad (\text{S5})$$

where  $\bar{\rho}_h$  is the mean density of the entire halo.

### The power-law density profile

For comparison, another commonly used model is a power-law density  $\rho_h(r) \sim r^{-m}$  with  $m = 2$  for isothermal density profile. We have

$$\rho_h(r) = (3-m) \frac{m_h}{4\pi r_h^3} \left( \frac{r}{r_h} \right)^{-m} = \frac{(3-m)m_r(r)}{4\pi r^3} = \frac{(3-m)}{3} \bar{\rho}_r(r), \quad (\text{S6})$$

and the density at halo surface is

$$\rho_h(r = r_h) = \frac{(3-m)m_h}{4\pi r_h^3}, \quad (\text{S7})$$

where  $m_r(r) = m_h(r/r_h)^{3-m}$ . For a power-law density, the halo density at radius  $r$  is fully determined by the mean density  $\bar{\rho}_r(r)$  of a sphere of radius  $r$  ( $\rho_h(r) \propto \bar{\rho}_r(r)$  from Eq. (S6)),

which is different from the NFW profile (See Eq. (S1)). This difference reflects the effect of mass cascade on the density profiles.

### The Einasto density profile

The third popular density profile was first introduced by Einasto to describe the distribution of stars within the Milky way [6],

$$\rho_h(r) = \rho_s e^{2/\alpha} \exp\left[-\frac{2}{\alpha} \left(\frac{r}{r_s}\right)^\alpha\right] \quad \text{and} \quad \frac{d \ln \rho_h}{d \ln r} = -2 \left(\frac{r}{r_s}\right)^\alpha, \quad (\text{S8})$$

where  $r_s$  is the scale radius (same as the NFW) that is defined as the location where the logarithmic slope is -2. The density  $\rho_s$  is defined as the halo density at scale radius  $r_s$ . The shape parameter  $\alpha$  is the exponent of the logarithmic slope in Eq. (S8). The mass  $m_r(r)$  can be obtained by the integration of density as,

$$m_r(r) = 4\pi \rho_s r_s^3 \frac{e^{2/\alpha}}{\alpha} \left(\frac{\alpha}{2}\right)^{3/\alpha} \left[ \Gamma\left(\frac{3}{\alpha}\right) - \Gamma\left(\frac{3}{\alpha}, \frac{2}{\alpha} \left(\frac{r}{r_s}\right)^\alpha\right) \right], \quad (\text{S9})$$

or equivalently in terms of the total halo mass  $m_h$ ,

$$m_r(r) = m_h \frac{\Gamma(3/\alpha) - \Gamma(3/\alpha, 2(r/r_s)^\alpha/\alpha)}{\Gamma(3/\alpha) - \Gamma(3/\alpha, 2c^\alpha/\alpha)}, \quad (\text{S10})$$

where  $\Gamma(x, y)$  is the upper incomplete gamma function. The Einasto density profile can be equivalently expressed in terms of the halo mass as,

$$\rho_h(r) = \frac{m_h}{4\pi r_h^3} \frac{c^3 \exp[-2(r/r_s)^\alpha/\alpha] \alpha (2/\alpha)^{3/\alpha}}{\Gamma(3/\alpha) - \Gamma(3/\alpha, 2c^\alpha/\alpha)} = \frac{\bar{\rho}_h(r) r^3 \exp[-2(r/r_s)^\alpha/\alpha] \alpha (2/\alpha)^{3/\alpha}}{3r_s^3 \Gamma(3/\alpha) - \Gamma(3/\alpha, 2(r/r_s)^\alpha/\alpha)}. \quad (\text{S11})$$

The density at the surface of halo is

$$\rho_h(r_h) = \frac{m_h}{4\pi r_h^3} \frac{c^3 \exp(-2c^\alpha/\alpha) \alpha (2/\alpha)^{3/\alpha}}{\Gamma(3/\alpha) - \Gamma(3/\alpha, 2c^\alpha/\alpha)}. \quad (\text{S12})$$

Same as the NFW profile, the halo density at radius  $r$  cannot be fully determined by the mean density  $\bar{\rho}_r(r)$  for the sphere of radius  $r$  (Eq. (S11)), which reflects the effect of mass cascade.

The Einasto profile has three free parameters ( $\rho_s$ ,  $r_s$ , and  $\alpha$ ) compared to the NFW profile ( $r_s$  and  $c$ ) with two free parameters. However, if the halo density at the surface is required to be the same for two different profiles (Eqs. (S5) and (S12)), we will have an additional implicit relation between the shape parameter  $\alpha$  and the halo concentration  $c$ ,

$$c \left( \ln(1+c) - \frac{c}{1+c} \right) (1+c)^2 = \frac{\Gamma(3/\alpha) - \Gamma(3/\alpha, 2c^\alpha/\alpha)}{\exp(-2c^\alpha/\alpha) \alpha (2/\alpha)^{3/\alpha}}. \quad (\text{S13})$$

Supplementary Fig. S1 plots the variation of shape parameter  $\alpha$  with concentration parameter  $c$  (of a NFW profile) by numerically solving Eq. (S13). Note that there is a discontinuity at around  $c=2$ . The shape parameter  $\alpha$  decreases from 0.2 to 0.155 for concentration parameter  $c$  varying from 4 to 10, i.e.  $\alpha$  increases with increasing mass that is consistent with simulations [7].

### Simple closures for self-consistent particle distribution

The inverse mass cascade leads to the random variation of halo size that gives rise to the “diffusion” motion of collisionless particles (Eqs. (122) and (123)). The osmotic velocity is the velocity acquired by particles to balance the external force and can be related to the flux of “diffusion”. A simple model of the osmotic velocity  $u_h^*(x)$  was proposed (Eq. (136)) to derive the particle probability function  $P_r(x)$  and halo density profile (Eq. (139) and (143)). The relation

between the radial flow  $u_h(x)$  and osmotic velocity  $u_h^*(x)$  is also presented in Eq. (129). The distribution function  $P_r(x)$  is fully determined if an additional closure can be introduced between  $u_h(x)$  and  $u_h^*(x)$ , which is the focus of this section.

In standard Brownian motion, a spherical particle of radius  $a_B$  moving at a constant velocity  $u_h$  in a fluid of viscosity  $\eta_B$  subject to a force  $F_B$  can be described by the Stokes' law. Therefore, the local steady-state velocity  $u_h$  can be fully determined by the driving force  $F_B$ , i.e. the gradient of the osmotic pressure  $\Pi_B = \rho_B k_B T$  ( $k_B$  is the Boltzmann constant and  $T$  is temperature), which is a localized short-range force. The current velocity  $u_h$  and osmotic velocity  $u_h^*$  can be written as,

$$u_h = \frac{F_B}{6\pi\eta_B a_B} = -\frac{1}{6\pi\eta_B a_B} \cdot \frac{1}{\rho_B} \frac{\partial \Pi_B}{\partial x} = -\frac{\mu_B}{\rho_B} \frac{\partial \Pi_B}{\partial x}$$

and

$$u_h^* = D_B \frac{\partial \ln \rho_B}{\partial x}, \quad (\text{S14})$$

where  $\rho_B$  is the particle number density,  $D_B$  is the particle diffusivity, and  $\mu_B$  is the particle mobility. The stochastic equations for Brownian motion (forward and backward) read

$$\frac{dr_t}{dt} = [u_h(x_t) + u_h^*(x_t)] + \sqrt{2D_B} \xi(t), \quad (\text{S15})$$

$$\frac{dr_t}{dt} = [u_h(x_t) - u_h^*(x_t)] + \sqrt{2D_B} \xi^*(t). \quad (\text{S16})$$

The corresponding Fokker-Planck equations read

$$\frac{\partial P_r(x, t)}{\partial t} = -\frac{\partial}{\partial x} [(u_h(x) + u_h^*(x)) P_r] + D_B \frac{\partial^2 P_r}{\partial x^2}, \quad (\text{S17})$$

$$\frac{\partial P_r(x, t)}{\partial t} = -\frac{\partial}{\partial x} [(u_h(x) - u_h^*(x)) P_r] - D_B \frac{\partial^2 P_r}{\partial x^2}. \quad (\text{S18})$$

The simple closure  $u_h = -u_h^*$  for Brownian motion is well known as the flux due to applied force  $F_B$  must balance the diffusive flux. The Einstein relation  $D_B = \mu_B k_B T$  is a direct result of this closure (Eqs (S14)). For Brownian motion with closure  $u_h = -u_h^*$ , the diffusion equation for particle probability  $P_r$  can be directly derived from Fokker-Planck equation (Eq. (S17)).

However, it is different and much more complicated for halos formed in self-gravitating collisionless flow (SG-CFD). In contrast to the Brownian motion, the osmotic velocity  $u_h^*(r)$  may not be fully determined by the local current velocity  $u_h(r)$  at location  $r$  due to the long-range and non-local nature of the gravitational force. Let's first derive the radial linear momentum within an arbitrary radius  $r$  for a given unknown function  $F(x)$ . With expressions of  $u_r$  (from Eq. (25) and  $\rho_h$  (from Eq.(16)), this can be obtained as,

$$L_{hr}(r) = \int_0^r u_r(r_1) 4\pi r_1^2 \rho_h(r_1, a) dr_1 = \frac{m_h r_s}{t F(c)} \left( x F(x) - 2 \int_0^x F(x) dx \right). \quad (\text{S19})$$

Due to the long-range interaction, the current velocity  $u_r(r_1)$  of every single spherical shell with radius  $r_1 < r$  should contribute to the osmotic velocity  $u_h^*(r)$  at radius  $r$ . Therefore,  $u_h^*(r)$  is proposed to be proportional to the mean radial velocity within a sphere of radius  $r$ ,

$$u_h^* \frac{r_s}{t} = \lambda_h \frac{L_{hr}(r)}{m_r(r)} = \frac{\lambda_h}{m_r(r)} \int_0^r u_r(r_1) 4\pi r_1^2 \rho_h(r_1, a) dr_1, \quad (\text{S20})$$

where  $\lambda_h$  is a proportional constant and  $m_r(r)$  is the halo mass within radius  $r$  (Eq. (15)). The final expression for osmotic velocity reads (using Eq. (S19)),

$$u_h^*(x) = \lambda_h \left[ x - \frac{2}{F(x)} \int_0^x F(y) dy \right]. \quad (\text{S21})$$

A third order differential equation for  $F(x)$  can be obtained by combining two closures Eqs. (S21) and (129),

$$F'''(x) + \frac{F''(x)F'(x)}{F(x)} + \frac{2}{x}F''(x) - \frac{[F''(x)]^2}{F'(x)} + \left(2 + \frac{1}{d_h}\right)\frac{F'(x)}{x^2} + \left(2 - \frac{1}{d_h}\right)\frac{[F'(x)]^2}{xF(x)} = 0, \quad (\text{S22})$$

where  $\sigma(x) = x^{\lambda_r} = x$  is used with  $\lambda_r = 1$ . Parameter  $d_h = d_r/\lambda_h$  lumps  $d_r$  and  $\lambda_h$  together. The associated boundary conditions are

$$F(0) = 0, \quad F(\infty) = 1, \quad (\text{S23})$$

$$F''(1) = 0, \quad \text{and} \quad \lim_{x \rightarrow 0} \frac{\partial u_h}{\partial x} = \lim_{x \rightarrow 0} \frac{F(x)F''(x)}{[F'(x)]^2} = \gamma_h. \quad (\text{S24})$$

Complete solution of  $F(x)$  from Eq. (S22) gives rise to the halo density profile and all other relevant quantities. By introducing a set of new variables  $y_1$ ,  $y_2$ , and  $x_1$ , where

$$y_1 = \ln F(x), \quad y_2 = \ln F'(x), \quad \text{and} \quad x_1 = \ln x, \quad (\text{S25})$$

the original Eq. (S22) can be equivalently reduced to two coupled equations

$$\frac{\partial^2 y_2}{\partial x_1^2} + \frac{\partial y_2}{\partial x_1} \left( \frac{\partial y_1}{\partial x_1} + 1 \right) + \left( 2 - \frac{1}{d_h} \right) \frac{\partial y_1}{\partial x_1} + \left( 2 + \frac{1}{d_h} \right) = 0, \quad (\text{S26})$$

$$\frac{\partial y_1}{\partial x_1} = \exp(y_2 - y_1 + x_1), \quad (\text{S27})$$

with corresponding boundary conditions,

$$\left. \frac{\partial y_1}{\partial x_1} \right|_{-\infty} = \frac{1}{1 - \gamma_h} \quad \text{and} \quad y_1|_{\infty} = 0, \quad (\text{S28})$$

$$\left. \frac{\partial y_2}{\partial x_1} \right|_{-\infty} = \frac{\gamma_h}{1 - \gamma_h} \quad \text{and} \quad \left. \frac{\partial y_2}{\partial x_1} \right|_0 = 0. \quad (\text{S29})$$

For small  $x_1 \rightarrow 0$  with power-law solution  $F(x) \propto x^{n_1}$ ,

$$\frac{\partial y_2}{\partial x_1} \equiv \frac{\partial y_1}{\partial x_1} - 1, \quad \frac{\partial^2 y_2}{\partial x_1^2} = 0 \quad \text{and} \quad n_1 = \frac{1}{2} \left[ \left( \frac{1}{d_h} - 2 \right) \pm \sqrt{\frac{1}{d_h} \left( \frac{1}{d_h} - 8 \right)} \right], \quad (\text{S30})$$

where we have  $d_h = 1/8$  for  $n_1 = 3$  (Table 3), which corresponds to density profile with a central core. For large  $x_1 \rightarrow \infty$  with  $F(x) \rightarrow 1$  or  $y_1 \rightarrow 0$  and  $\partial y_1 / \partial x_1 \ll 1$ , the simplified equation and a power-law solution of  $F'(x) \propto x^{n_2}$  can be obtained (from Eq. (S26)),

$$\frac{\partial^2 y_2}{\partial x_1^2} + \frac{\partial y_2}{\partial x_1} + \left( 2 + \frac{1}{d_h} \right) = 0 \quad \text{and} \quad n_2 = - \left( 2 + \frac{1}{d_h} \right). \quad (\text{S31})$$

With  $d_h = 1/8$ ,  $F'(x) \propto x^{-10}$  for  $x_1 \rightarrow \infty$ .

More study is required to identify other non-local closure between  $u_h(x)$  and  $u_h^*(x)$ . The other option is to use the equation of state for relative pressure and density as a simple closure. For virialized halos with vanishing radial flow (no term 2 in Eq. (61)), the hydrostatic equilibrium equation

$$\frac{d}{dr} \left( \frac{r^2}{\rho_h} \frac{dp_h}{dr} \right) = -4\pi G r^2 \rho_h(r) \quad (\text{S32})$$

can be used to relate the pressure to density. Assuming equation of state (157) is valid for entire virialized halo and inserting it into the hydrostatic equilibrium equation,

$$K_s b_r \frac{d}{dr} \left( r^2 \frac{(\rho_h(0) - \rho_h)^{b_r-1}}{\rho_h} \frac{d\rho_h}{dr} \right) = -4\pi G r^2 \rho_h. \quad (\text{S33})$$

This model leads to an isothermal density profile  $\rho_h \propto r^{-2}$  for large  $r$  with  $\rho_h(r) \rightarrow 0$  and an Einasto profile for small  $r$  with a central core. Equation (160) may also be modified with a density dependent exponent of equation of state,



$$\Delta p_{hn} = K_1 (\Delta \rho_{hn})^{b_r \left( \frac{\rho_h(x)}{\rho_h(0)} \right)^n}. \quad (\text{S34})$$

With this closure and Eqs. (158) and (159) for  $\Delta p_{hn}$  and  $\Delta \rho_{hn}$ , the unknown function  $F(x)$  can be fully determined. Further study is needed for a self-consistent particle distribution function that will provide fundamental understanding of halo internal structures.

## Supplementary figures

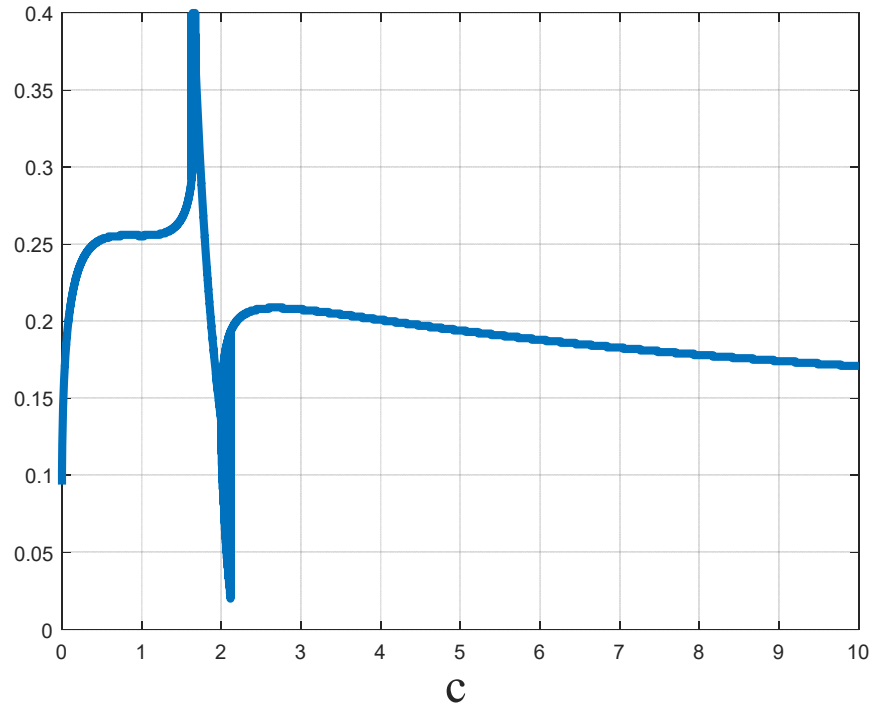


Figure S1. The variation of shape parameter  $\alpha$  of an Einasto profile with the concentration parameter  $c$  of NFW profile. Both NFW and Einasto profiles are assumed to have the same density at halo surface by numerically solving Eq. (S13). Note that there is a discontinuity at  $c=2$ . Parameter  $\alpha$  is on the order of 0.2 and slowly decreases with increasing  $c$  toward small halos.

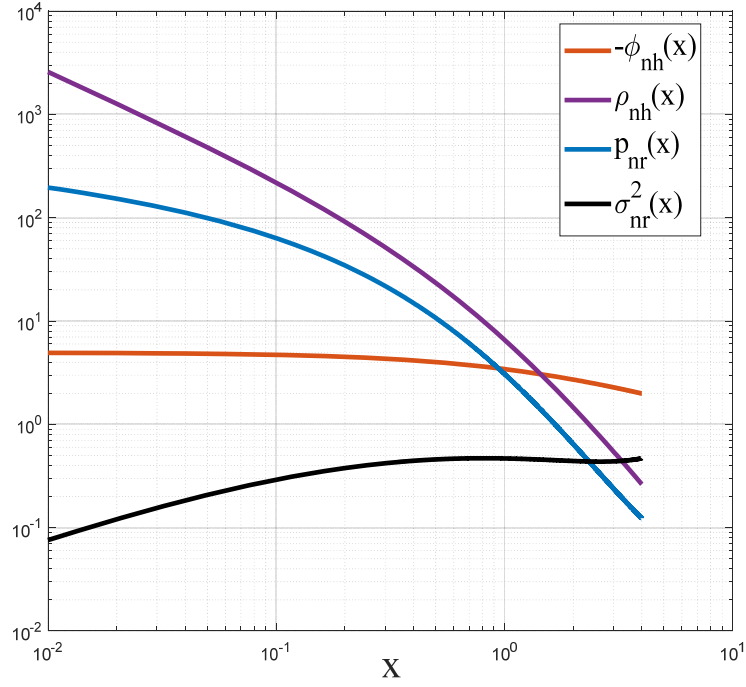


Figure S2. The variation of normalized pressure  $p_{\text{nr}}(x)$ , gravitational potential  $\phi_{\text{nh}}(x)$  and radial velocity dispersion  $\sigma_{\text{nr}}^2(x)$  for a NFW profile with  $c = 4$  (Eqs. (69)-(72)) and a nonzero radial flow. The halo density  $\rho_{\text{nh}}(x)$  is normalized by halo mean density  $\bar{\rho}_h$ .

## References

1. C. S. Frenk, et al., *Public Release of N-body simulation and related data by the Virgo consortium*. arXiv:astro-ph/0007362v1 2000.
2. Jenkins, A., et al., *Evolution of structure in cold dark matter universes*. Astrophysical Journal, 1998. **499**(1): p. 20.
3. Colberg, J.M., et al., *Linking cluster formation to large-scale structure*. Monthly Notices of the Royal Astronomical Society, 1999. **308**(3): p. 593-598.
4. Sheth, R.K., H.J. Mo, and G. Tormen, *Ellipsoidal collapse and an improved model for the number and spatial distribution of dark matter haloes*. Monthly Notices of the Royal Astronomical Society, 2001. **323**(1): p. 1-12.
5. Navarro, J.F., C.S. Frenk, and S.D.M. White, *A universal density profile from hierarchical clustering*. Astrophysical Journal, 1997. **490**(2): p. 493-508.
6. Einasto, J., et al., *Structure of Superclusters and Supercluster Formation .3. Quantitative Study of the Local Supercluster*. Monthly Notices of the Royal Astronomical Society, 1984. **206**(3): p. 529-558.
7. Gao, L., et al., *The redshift dependence of the structure of massive Lambda cold dark matter haloes*. Monthly Notices of the Royal Astronomical Society, 2008. **387**(2): p. 536-544.